A transient role of primary cilia in controlling direct versus indirect neurogenesis in the developing cerebral cortex

Kerstin Hasenpusch-Theil[1], Christine Laclef[2,3], Matt Colligan[1], Eamon Fitzgerald[1], Katherine Howe[1], Emily Carroll[1], Shaun R. Abrams[4], Jeremy F. Reiter[4,5], Sylvie Schneider-Maunoury[2], and Thomas Theil[1,6]

[1]Centre for Discovery Brain Sciences, Hugh Robson Building, University of Edinburgh, Edinburgh, EH8 9XD, United Kingdom

[2] Sorbonne Université, CNRS UMR7622, INSERM U1156, Institut de Biologie Paris Seine (IBPS) - Developmental Biology Unit, 75005, Paris, France

[3]Present address: Sorbonne Université, Institut du Fer à Moulin INSERM U1270, Paris, France

[4]Department of Biochemistry and Biophysics, University of California, San Francisco, CA 94143

[5]Chan Zuckerberg Biohub, San Francisco, CA94158, USA Chan Zuckerberg Biohub, San Francisco, CA 94158, USA

[6]Author for correspondence (email: thomas.theil@ed.ac.uk)

Running title: Inpp5e and direct/indirect neurogenesis

Key words: *Inpp5e*; *Tctn2*; primary cilia; neurogenesis; cortex

ABSTRACT

During the development of the cerebral cortex, neurons are generated directly from radial glial cells or indirectly via basal progenitors. The balance between these division modes determines the number and types of neurons formed in the cortex thereby affecting cortical functioning. Here, we investigate the role of primary cilia in this process. We show that a mutation in the ciliary gene *Inpp5e* leads to a transient increase in direct neurogenesis and subsequently to an overproduction of layer V neurons in newborn mice. Loss of *Inpp5e* also affects ciliary structure coinciding with increased Akt and mTOR signalling and reduced Gli3 repressor levels. Genetically re-storing Gli3 repressor rescues the decreased indirect neurogenesis in *Inpp5e* mutants. Overall, our analyses reveal how primary cilia determine neuronal subtype composition of the cortex by controlling direct vs indirect neurogenesis. These findings have implications for understanding cortical malformations in ciliopathies with *INPP5E* mutations.

INTRODUCTION

Building a functional cerebral cortex which confers humans with their unique cognitive capabilities requires controlling the proliferation of neural progenitor cells and the timing and modes of neurogenic cell divisions. Varying the timing and modes of neurogenesis affects neuronal numbers and subtype composition of the cortex (Florio & Huttner, 2014). In the developing murine cortex, radial glial cells (RGCs) represent the major neural stem cell type. Residing in the ventricular zone, they express Pax6 and undergo interkinetic nuclear migration dividing at the ventricular surface (Götz, Stoykova, & Gruss, 1998; Warren et al., 1999). Initially, RGCs go through rounds of symmetric proliferative divisions to produce two RGCs increasing the progenitor pool but switch to asymmetric divisions at the beginning of cortical neurogenesis. RGCs generate neurons in two ways, either directly or indirectly via the production of basal progenitors (BPs) that settle in the subventricular zone (SVZ) and express the Tbr2 transcription factor (Englund et al., 2005). In the mouse, the majority of BPs divide once to produce two neurons whereas the remainders undergo one additional round of symmetric proliferative division before differentiating into two neurons (Haubensak, Attardo, Denk, & Huttner, 2004; Miyata et al., 2004; Noctor, Martinez-Cerdeno, Ivic, & Kriegstein, 2004). In this way, BPs increase neuron output per radial glial cell and have therefore been implicated in the evolutionary expansion of the mammalian cerebral cortex (Martinez-Cerdeno, Noctor, & Kriegstein, 2006). Thus, the balance between direct and indirect neurogenesis is an important factor in generating appropriate neuron numbers and types.

The mechanisms that fine tune this balance and thereby adjust the numbers and types of neurons produced in the cortex have only recently been investigated. Mitotic spindle orientation (Postiglione et al., 2011) and endoplasmic reticulum (ER) stress (Gladwyn-Ng et al., 2018; Laguesse et al., 2015) are contributing factors to control the generation of basal progenitors. In addition, levels of Slit/Robo and Notch/Delta signaling were shown to be evolutionarily conserved factors that determine the predominant mode of neurogenesis (Cardenas et al., 2018). Moreover, feedback signals from postmitotic neurons control the fate of radial glial daughter cells involving the release of Neurotrophin-3 and Fgf9 (Parthasarathy, Srivatsa, Nityanandam, & Tarabykin, 2014; Seuntjens et al., 2009) as well as the activation of a Notch-dependent signaling pathway (W. Wang et al., 2016). These studies highlight the importance of cell-cell signaling in controlling the cell lineage of cortical progenitors (Silva, Peyre, & Nguyen, 2019) and emphasize the necessity of studying the cellular mechanisms by which these signals control the decision by RGCs to undergo direct or indirect neurogenesis.

Given the importance of cell-cell signaling, it is likely that the primary cilium, a signaling hub in embryogenesis in general and in neural development in particular (Valente, Rosti, Gibbs, & Gleeson, 2014), plays key roles in determining the balance between direct versus indirect neurogenesis. The cilium is a subcellular protrusion that predominately emanates from the apical surface of radial glial cells projecting into the ventricular lumen. The phenotypes of several mouse

80 lines mutant for ciliary genes underline the importance of the primary cilium in forebrain development
81 but these mutants often suffer from severe patterning defects (Ashique et al., 2009; Besse et al.,
82 2011; Willaredt et al., 2008) which make studying ciliary roles in determining the lineage of cortical
83 progenitors difficult. To address such functions, we investigated corticogenesis in a mouse mutant
84 for the ciliary gene *Inpp5e*.

85 *INPP5E* is mutated in Joubert syndrome (JS) (Bielas et al., 2009; Jacoby et al., 2009), a
86 ciliopathy characterized by cerebellar defects in which a subset of patients also shows malformations
87 of the cerebral cortex including heterotopias, polymicrogyria and agenesis of the corpus callosum
88 (Valente et al., 2014). *Inpp5e* encodes Inositol polyphosphate 5 phosphatase E, an enzyme that is
89 localized in the ciliary membrane and that hydrolyses the phosphatidylinositol polyphosphates
90 $PI(4,5)P_2$ and $PI(3,4,5)P_3$ (Bielas et al., 2009; Jacoby et al., 2009). In this way, it controls the inositol
91 phosphate composition of the ciliary membrane and thereby regulates the activity of several
92 signaling pathways and cilia stability (Bielas et al., 2009; Chavez et al., 2015; Garcia-Gonzalo et al.,
93 2015; Jacoby et al., 2009; Plotnikova et al., 2015). In contrast to *Inpp5e*'s extensively studied
94 biochemical and cellular roles, little is known how these diverse functions are employed at the tissue
95 level to control RGC lineage.

96 Here, we show that loss of *Inpp5e* function results in an increase in neuron formation at the
97 expense of basal progenitor production in the E12.5 cortex and in an overproduction of Ctip2+ layer
98 V neurons in newborn mutants. Moreover, RGC cilia show unusual membranous structures and/or
99 abnormal numbers of microtubule doublets affecting the signaling capabilities of the cilium. The
100 levels of Gli3 repressor (Gli3R), a critical regulator of cortical stem cell development (Hasenpusch-
101 Theil et al., 2018; H. Wang, Ge, Uchida, Luu, & Ahn, 2011), is reduced and re-introducing Gli3R
102 rescues the decreased formation of basal progenitors. Taken together, these findings implicate the
103 primary cilium in controlling the decision of RGCs to either undergo direct neurogenesis or to form
104 basal progenitors, thereby governing the neuronal subtype composition of the cerebral cortex.
105

106 **RESULTS**

107

108 ***Inpp5e*$^{\Delta/\Delta}$ embryos show mild telencephalic patterning defects**

109 Controlling the balance between direct and indirect neurogenesis in the developing cerebral
110 cortex is mediated by cell-cell signaling (Cardenas et al., 2018) and is hence likely to involve the
111 primary cilium. To investigate potential ciliary roles, we started characterizing cortical stem cell
112 development in embryos mutant for the *Inpp5e* gene which has a prominent role in ciliary signaling
113 and stability. Mutations in ciliary genes have previously been found to result in telencephalon
114 patterning defects, most notably in a ventralisation of the dorsal telencephalon and/or in defects at
115 the corticoseptal (CSB) and pallial/subpallial boundaries (PSPB) (Ashique et al., 2009; Besse et al.,
116 2011; Willaredt et al., 2008). Therefore, we first considered the possibility that such early patterning
117 defects may be present in *Inpp5e* mutant embryos and could affect cortical stem cell development.
118 In situ hybridization and immunofluorescence analyses of E12.5 control and *Inpp5e*$^{\Delta/\Delta}$ embryos
119 revealed no obvious effect on the expression of dorsal and ventral telencephalic markers at the
120 corticoseptal boundary (SupFig. 1). In contrast, the pallial/subpallial boundary was not well defined
121 with a few scattered Pax6+ and *Dlx2* expressing cells on the wrong side of the boundary, i.e. in the
122 subpallium and pallium, respectively (SupFig. 1). Moreover, the hippocampal anlage appeared
123 smaller and disorganized with low level and diffuse expression of cortical hem markers (SupFig. 2),
124 consistent with known roles of Wnt/β-catenin and Bmp signaling in hippocampal development
125 (Galceran, Miyashita-Lin, Devaney, Rubenstein, & Grosschedl, 2000; Lee, Tole, Grove, & McMahon,
126 2000). In contrast, progenitors in the neocortical ventricular zone of *Inpp5e* mutant mice expressed
127 the progenitor markers *Emx1*, *Lhx2*, *Pax6* and *Ngn2,* though the levels of Pax6 protein expression
128 appeared reduced in the medial neocortex suggestive of a steeper lateral to medial Pax6 expression
129 gradient in mutant embryos. These expression patterns were maintained in E14.5 *Inpp5e*$^{\Delta/\Delta}$ embryos
130 but revealed an area in the very caudal/dorsal telencephalon where the neocortex was folded
131 (SupFig. 3). At this level, folds were also present in the hippocampal anlage. Taken together, these
132 findings indicate that *Inpp5e* mutants have mild patterning defects affecting the integrity of the PSPB,
133 hippocampal development and the caudal-most neocortex while the rostral neocortex shows no
134 obvious malformation and can therefore be analysed for effects of the *Inpp5e* mutation on direct and
135 indirect neurogenesis.

136

137 ***Inpp5e* controls direct vs indirect neurogenesis in the lateral neocortex**

138 Based upon these findings, we started analyzing the proliferation and differentiation of radial
139 glial cells in *Inpp5e*$^{\Delta/\Delta}$ embryos in the rostrolateral and rostromedial neocortex to avoid the
140 regionalization defects described above. As a first step, we determined the proportion of radial glial
141 cells, basal progenitors and neurons in these regions in E12.5 embryos. Double
142 immunofluorescence for PCNA which labels all progenitor cells (Hall et al., 1990) and the radial glial

143 marker Pax6 did not reveal differences in the proportions of radial glial cells at both medial and lateral
144 levels (Fig. 1A-D). In contrast, the proportion of Tbr2+ basal progenitors was reduced laterally but
145 not medially (Fig. 1E-H). This decrease coincided with an increase in Tbr1+ neurons specifically in
146 the lateral neocortex (Fig. 1I-L). To determine whether these alterations are maintained at a later
147 developmental stage, we repeated this investigation in E14.5 embryos. This analysis revealed no
148 significant differences in the proportion of Pax6+ RGCs (Fig. 2A-D). Similarly, there was no alteration
149 in the proportion of Tbr2+ basal progenitors in lateral neocortex, however, their proportion was
150 reduced medially (Fig. 2E-H).

151 To label cortical projection neurons, we used double immunofluorescence for Tbr1 and Ctip2
152 which allowed us to distinguish between Ctip2+Tbr1+ and Ctip2+Tbr1- neurons. Quantifying these
153 subpopulations showed no effect on the formation of Ctip2+Tbr1+ neurons in *Inpp5e*$^{\Delta/\Delta}$ embryos. In
154 contrast, the proportion of Ctip2+Tbr1- neurons was reduced medially but increased in the lateral
155 neocortex (Fig. 2I-R). Taken together, these findings show that initially Tbr1+ and later Ctip2+Tbr1-
156 neurons were increasingly formed in the lateral neocortex of *Inpp5e*$^{\Delta/\Delta}$ embryos and that the
157 proportion of basal progenitors recovered after an initial down-regulation.

158 To address the defective cellular processes underlying these neurogenesis defects in *Inpp5e*
159 mutants, we first measured proliferation rates of cortical progenitors and performed double
160 immunofluorescence for PCNA and pHH3 which labels mitotic radial glial cells located at the
161 ventricular surface and dividing basal progenitors in abventricular positions (SupFig. 4). This analysis
162 revealed no statistically significant differences in the E12.5 and E14.5 lateral neocortex of control
163 and *Inpp5e*$^{\Delta/\Delta}$ embryos. The proportion of mitotic basal progenitors, however, was reduced in the
164 E12.5 medial neocortex (SupFig. 4).

165 The cell cycle represents another key regulator of neuronal differentiation and a mutation in
166 *Kif3a* affects ciliogenesis and the cell cycle in the developing neocortex (Wilson, Wilson, Wang,
167 Wang, & McConnell, 2012). To investigate the possibility of altered cell cycle kinetics, we used a
168 BrdU/IdU double labelling strategy (Martynoga, Morrison, Price, & Mason, 2005; Nowakowski,
169 Lewin, & Miller, 1989) to determine S phase length and total cell cycle length in radial glial cells and
170 found no statistically significant changes in these parameters (SupFig. 5).

171 Finally, the increased neuron production could also be explained by an increase in direct
172 neurogenesis at the expense of basal progenitor cell formation. To test this possibility, we gave BrdU
173 to E11.5 pregnant mice 24h before dissecting the embryos. We then used BrdU immunostaining in
174 conjunction with Tbr1 and Tbr2 to identify the neurons and basal progenitors formed in the lateral
175 neocortex within the 24h time period. This analysis showed that the proportion of Tbr1+ neurons
176 compared to the total number of BrdU+ cells increased while the Tbr2+ proportion decreased in
177 *Inpp5e* mutants (Fig. 3). Since the cell cycle of basal progenitors is longer than 24h (Arai et al.,
178 2011), the 24h interval used in our cell cycle exit experiment was too short for newly formed basal
179 progenitors to undergo one additional round of the cell cycle and as the BrdU label would have been

180 diluted with a further round of division, this analysis supports our hypothesis that direct neurogenesis
181 became more prevalent in *Inpp5e*$^{\Delta/\Delta}$ radial glial cells.
182
183 **Cortical malformations in *Inpp5e*$^{\Delta/\Delta}$ embryos**
184 Next, we investigated the consequences of this increase in direct neurogenesis on cortical
185 size and layer formation. Since *Inpp5e*$^{\Delta/\Delta}$ newborn pups die perinatally (Bielas et al., 2009), we
186 focused our analysis on E18.5 embryos. The mutant lacked obvious olfactory bulbs, as revealed by
187 whole mounts of control and mutant brains (SupFig. 6). To gain insights into the overall histology of
188 the mutant forebrain, we stained coronal sections with DAPI. This analysis showed that the mutant
189 cortex was thinner laterally but not medially with a more pronounced reduction of the thickness at
190 caudal levels (SupFig. 7). In addition, the hippocampus was malformed with a smaller dentate gyrus.
191 Investigating the expression of markers characteristic of the entire hippocampus (*Nrp2*; (Galceran
192 et al., 2000)), the CA1 field (Scip1; (Frantz, Bohner, Akers, & McConnell, 1994)) and the dentate
193 gyrus (Prox1; (Oliver et al., 1993)) showed that these hippocampal structures were present but were
194 severely reduced in size and disorganized in *Inpp5e*$^{\Delta/\Delta}$ embryos (SupFig. 8). In addition, the corpus
195 callosum, the major axon tract connecting the two cerebral hemispheres, was correctly formed but
196 was smaller. We confirmed this effect by staining callosal axons and surrounding glial cells that guide
197 these axons to the contralateral hemisphere with L1 and GFAP, respectively (SupFig. 9).
198 After characterizing the gross morphology of the *Inpp5e*$^{\Delta/\Delta}$ cortex, we next investigated
199 whether the increased neuron formation in E12.5 mutant embryos led to changes in the neuronal
200 subtype composition of the E18.5 cortex. To this end, we used immunofluorescence labelling for
201 Tbr1 and Ctip2 to analyse the formation of layer VI and V neurons, respectively, whereas Satb2
202 served as a layer II-IV marker (Fig. 4). Inspecting these immunostainings at low magnification
203 showed that Tbr1+, Ctip2+ and Satb2+ neurons occupied their correct relative laminar positions in
204 *Inpp5e* mutants (Fig. 4A-F) except for neuronal heterotopias which were present in all mutant brains,
205 though their number and position varied (Fig. 4D). These immunostainings also revealed a medial
206 shift in the position of the rhinal fissure, a sulcus that is conserved across mammalian species and
207 separates neocortex from the paleocortical piriform cortex (Ariens-Kapers, Huber, & Crosby, 1936).
208 This shift was more marked caudally and suggests a dramatic expansion of the *Inpp5e* mutant
209 piriform cortex at the expense of neocortex at caudal most levels (Fig. 4D-F). Using the Tbr1/Ctip2
210 and Satb2 stainings, we determined the proportions of deep and superficial layer neurons,
211 respectively. Because of the expanded piriform cortex in *Inpp5e* mutants, we limited this
212 investigation to the unaffected rostral neocortex. In the rostrolateral neocortex, we found the
213 proportion of Tbr1+ neurons to be reduced (Fig. 4G, H, M). This reduction coincided with an
214 increased proportion of Ctip2+ layer V neurons (Fig. 4I, J, N) while the Satb2 population was
215 unchanged (Fig. 4K, L, O). In contrast, the rostromedial neocortex did not show any differences (Fig.

216 4P-X). Thus, the increase in direct neurogenesis in the lateral neocortex during earlier development
217 concurs with a change in the proportions of E18.5 Tbr1+ and Ctip2+ deep layer neurons.
218
219 **A mutation in the ciliary gene *Tctn2* leads to increased telencephalic neurogenesis**
220 To start to unravel the mechanisms by which *Inpp5e* controls cortical stem cell development,
221 we first analysed whether the increased early neurogenesis is restricted to *Inpp5e*$^{\Delta/\Delta}$ mutants or is
222 observed in another mutant affecting cilia. To this end, we focused on the *TECTONIC* 2 (*TCTN2*)
223 gene which is crucial for ciliary transition zone architecture (Shi et al., 2017) and which, like *INPP5E*,
224 is mutated in Joubert Syndrome (Garcia-Gonzalo et al., 2011). Interestingly, E12.5 *Tctn2*$^{-/-}$ mutant
225 embryos (Reiter & Skarnes, 2006) also showed an increased proportion of Tbr1+ projection neurons
226 and a concomitant decrease in Tbr2+ basal progenitors in the dorsolateral telencephalon (Fig. 5).
227 Due to embryonic lethality, however, we were not able to investigate the formation of cortical neurons
228 at later stages.
229
230 **Ciliary defects in the forebrain of E12.5 *Inpp5e*$^{\Delta/\Delta}$ embryos**
231 Our findings in the *Inpp5e* and *Tctn2* mutants suggested a role for cilia in cortical progenitor
232 cells to control early neurogenesis. Therefore, we examined the presence and the structure of
233 primary cilia in the developing forebrain of *Inpp5e*$^{\Delta/\Delta}$ embryos by immunofluorescence and electron
234 microscopy. We first analyzed the presence of the small GTPase Arl13b, enriched in ciliary
235 membranes, and of γ-Tubulin (γTub), a component of basal bodies (Caspary, Larkins, & Anderson,
236 2007). We found no major difference in the number, the apical localization or the size of cilia in
237 control and *Inpp5e*$^{\Delta/\Delta}$ neuroepithelial cells in the E12.5 telencephalon (Fig. 6A,B) or diencephalon
238 (data not shown).
239 To gain insights into the fine structure of these primary cilia we performed electron
240 microscopy analyses. Scanning electron microscopy (SEM) provided an observation of the cilia
241 protruding into the telencephalic ventricles. In control embryos, almost all radial glial cells had a
242 single, ~1 μm long primary cilium (Fig. 6C), as previously described (Besse et al., 2011). Some
243 *Inpp5e*$^{\Delta/\Delta}$ mutant cells also displayed an apparently normal cilium (Fig. 6D, E), whereas other cells
244 harbored abnormal cilia, either with a lateral blob (arrowhead in Fig. 6D) or as a short and bloated
245 cilium-like protrusion (arrows in Fig. 6D,E).
246 Transmission electron microscopy (TEM) confirmed the presence of abnormal cilia in
247 *Inpp5e*$^{\Delta/\Delta}$ embryos. Cilia were recognized by basal bodies anchored to the apical membrane in both
248 control and *Inpp5e*$^{\Delta/\Delta}$ radial glial cells (Fig. 6F-L, N, Q). However, in *Inpp5e*$^{\Delta/\Delta}$ cells, some cilia lacked
249 the axoneme and showed unusual membranous structures that resemble budding vesicles emerging
250 from the lateral surface of the cilium (Fig. 6G, K), internal vesicles (arrows in Fig. 6I, K, L), or
251 undulating peripheral membranes (Fig. 6I), indicating an *Inpp5e*-dependent defect in ciliary
252 membrane morphology. Transverse sections revealed the presence of cilia with apparently normal

253 9+0 axonemes, as well as cilia containing abnormal numbers of microtubule doublets in *Inpp5e*$^{\Delta/\Delta}$
254 embryos (Fig. 6O, P). To quantify these ciliary defects, we counted the number of normal versus
255 abnormal cilia on TEM images obtained from control and *Inpp5e*$^{\Delta/\Delta}$ embryos, and found an increase
256 in abnormal cilia in *Inpp5e*$^{\Delta/\Delta}$ compared to control embryos (Fig. 6R). Taken together, a significant
257 number of abnormal primary cilia were found at the apical end of E12.5 radial glial cells in the
258 forebrain of *Inpp5e*$^{\Delta/\Delta}$ embryos. These abnormalities are consistent with a role of *Inpp5e* in
259 maintaining cilia stability (Jacoby et al., 2009).
260
261 **Receptor tyrosine kinase and mTOR signaling in *Inpp5e*$^{\Delta/\Delta}$ embryos**
262 Given these defects in ciliary structure, we started to investigate cilia-controlled signaling
263 pathways, defects in which might underlie the increased direct neurogenesis in the *Inpp5e*$^{\Delta/\Delta}$ mutant
264 radial glial cells. Inpp5e hydrolyzes the 5-phosphate of PI(3,4,5)P_3 which serves as a second
265 messenger in receptor tyrosine kinase signaling. We therefore investigated the amount and
266 distribution of pErk1/2 as a read-out of receptor tyrosine kinase signaling. Western blots using
267 dissected dorsal telencephalon from E12.5 and E14.5 embryos revealed no difference in the ratio
268 between pErk1/2 and Erk1/2 (SupFig. 10). Moreover, pErk1/2 expression in the E12.5 forebrain
269 remains restricted to the LGE, the diencephalon and to meninges covering the telencephalon but
270 was not identified in cortical progenitors (SupFig. 10). In E14.5 embryos, we detected pErk1/2
271 immunoreactivity in cortical progenitors in a lateral to medial gradient covering the whole extent of
272 the neocortex. In contrast, high level pErk1/2 expression remained confined to the lateral neocortex
273 with little or no expression medially in *Inpp5e*$^{\Delta/\Delta}$ embryos (SupFig. 10). These findings suggest that
274 pErk signaling does not play a role in the early neurogenesis defect in *Inpp5e* mutants but may be
275 involved in the recovery of basal progenitor formation.
276 PI(3,4,5)P_3, a substrate of the Inpp5e phosphatase, is essential for the effective activation of
277 the serine threonine kinase Akt (Kisseleva, Cao, & Majerus, 2002; Plotnikova et al., 2015) raising
278 the possibility that loss of *Inpp5e* results in activated Akt signaling in the neocortex. Moreover,
279 phosphorylation of Akt at Serine^{473} has been implicated in inhibiting cilia assembly and promoting
280 cilia disassembly (Mao et al., 2019). We therefore investigated the amount of phospho-Akt^{S473} in
281 western blots on protein extracts from the E12.5 and E14.5 dorsal telencephalon. This analysis
282 revealed increased phosphorylation of Akt at Serine^{473} at E12.5 but no significant change at E14.5
283 (SupFig. 11). Since Akt acts upstream of mTOR (Yu & Cui, 2016), we also analysed the activity of
284 the mTOR pathway and investigated the phosphorylation of the S6 ribosomal protein, at Serine$^{235/236}$
285 and Serine$^{S240/244}$ (Ferrari, Bandi, Hofsteenge, Bussian, & Thomas, 1991). Interestingly, *Inpp5e*
286 mutants showed increased S6 phosphorylation at Serine$^{235/236}$ in E12.5 and E14.5 embryos whereas
287 an increase in phospho-S6$^{S240/244}$ remained restricted to E12.5 (SupFig. 11). Taken together, these
288 findings indicate that *Inpp5e* inactivation leads to increased activation of Akt and mTOR signaling in
289 the E12.5 dorsal telencephalon.

290 Next, we investigated a potential role of elevated mTOR signaling in controlling the balance
291 between direct and indirect neurogenesis and treated E11.5 pregnant mice with the mTORC1
292 inhibitor rapamycin (1mg/kg bodyweight). We harvested embryos 24h later and determined the
293 proportions of basal progenitors and neurons. This analysis revealed that administering rapamycin
294 did not rescue basal progenitor and neuron formation although the cortex of rapamycin treated
295 *Inpp5e*$^{\Delta/\Delta}$ embryos appeared elongated (SupFig. 11). Based on this experiment, augmented mTOR
296 signaling does not underlie the altered ratio of direct vs indirect neurogenesis in *Inpp5e*$^{\Delta/\Delta}$ embryos.
297

298 **Restoring Gli3 repressor ratio rescues cortical malformations in *Inpp5e*$^{\Delta/\Delta}$ embryos**

299 Primary cilia also play a crucial role in Shh signaling by controlling the proteolytic cleavage
300 of full length Gli3 (Gli3FL) into the Gli3 repressor form (Gli3R) in the absence of Shh and by
301 converting Gli3FL into the transcriptional activator Gli3A in the presence of Shh. Moreover, the dorsal
302 telencephalon predominately forms Gli3R (Fotaki, Yu, Zaki, Mason, & Price, 2006) and mice that
303 can only produce Gli3R have no obvious defect in cortical development (Besse et al., 2011; Böse,
304 Grotewold, & Rüther, 2002). In addition, we recently showed that Gli3 has a prominent role in radial
305 glial cells controlling the switch from symmetric proliferative to asymmetric neurogenic cell division
306 (Hasenpusch-Theil et al., 2018). Therefore, we hypothesized that alterations in Gli3 processing
307 caused by abnormal cilia function underlies the increased direct neurogenesis and the cortical
308 malformations in *Inpp5e*$^{\Delta/\Delta}$ embryos. In situ hybridization showed that *Gli3* mRNA expression might
309 be slightly reduced but the overall expression pattern in the telencephalon remains unaffected
310 (SupFig. 12). We next investigated the formation of Gli3FL and Gli3R in the E12.5 dorsal
311 telencephalon of *Inpp5e*$^{\Delta/\Delta}$ embryos using Western blots. This analysis revealed no change in the
312 levels of Gli3FL but a significant decrease inGli3R which resulted in a reduced Gli3R to Gli3FL ratio
313 in the mutant (Fig. 7A-D) suggesting that the *Inpp5e* mutation affects Gli3 processing.

314 The next set of experiments aimed to clarify a role for the reduced Gli3 processing. To this
315 end, we restored Gli3R levels by crossing *Inpp5e* mutants with *Gli3*$^{\Delta 699/+}$ mice that can only produce
316 Gli3R in a cilia-independent manner (Besse et al., 2011; Böse et al., 2002). Overall inspection of
317 *Inpp5e*$^{\Delta/\Delta}$;*Gli3*$^{\Delta 699/+}$ embryos revealed normal eye formation whereas *Inpp5e*$^{\Delta/\Delta}$ embryos either
318 completely lacked eyes or showed microphthalmia (Jacoby et al., 2009) (SupFig. 13). Moreover, the
319 overall morphology of the telencephalon is much improved in *Inpp5e*$^{\Delta/\Delta}$;*Gli3*$^{\Delta 699/+}$ embryos as
320 compared to *Inpp5e*$^{\Delta/\Delta}$ embryos. In E18.5 *Inpp5e*$^{\Delta/\Delta}$ *Gli3*$^{\Delta 699/+}$ mutants, the corpus callosum has a
321 thickness indistinguishable from that of control embryos (SupFig. 14). In E12.5 and E14.5
322 *Inpp5e*$^{\Delta/\Delta}$;*Gli3*$^{\Delta 699/+}$ embryos, the neocortex lacks the undulations of the VZ present in *Inpp5e*$^{\Delta/\Delta}$
323 embryos (data not shown) and the morphology of the hippocampal anlage is more akin to that in
324 wild-type embryos but it is still smaller and less bulged (Fig. 7E, H, K, N).

325 We also determined the proportions of basal progenitors and Tbr1+ neurons at E12.5 which
326 were decreased and increased, respectively, in the lateral neocortex of *Inpp5e*$^{\Delta/\Delta}$ embryos.

327 Remarkably, there was no statistically significant difference between control and *Inpp5e*$^{\Delta/\Delta}$;*Gli3*$^{\Delta699/+}$
328 embryos (Fig. 7E-J) indicating that the neurogenesis phenotype of E12.5 *Inpp5e*$^{\Delta/\Delta}$ mutants is
329 rescued by a single copy of the Gli3$^{\Delta699}$ allele. The proportion of Tbr1+Ctip2+ neurons was not
330 affected in the medial neocortex of E14.5 *Inpp5e*$^{\Delta/\Delta}$;*Gli3*$^{\Delta699/+}$ embryos (Fig. 7K, M, N) either, however,
331 the proportion of Tbr1-Ctip2+ neurons was reduced (Fig. 7K, N, P). Similarly, the proportions of basal
332 progenitors in the E14.5 medial neocortex was reduced in *Inpp5e*$^{\Delta/\Delta}$ *Gli3*$^{\Delta699/+}$ embryos as in *Inpp5e*$^{\Delta/\Delta}$
333 embryos (Fig. 7L, O, S). As re-introducing a single Gli3$^{\Delta699}$ allele does not completely rescue the
334 *Inpp5e*$^{\Delta/\Delta}$ neurogenesis phenotype, we generated *Inpp5e*$^{\Delta/\Delta}$ embryos homozygous for Gli3$^{\Delta699}$.
335 Interestingly, the morphology of the telencephalon including the hippocampal formation was
336 indistinguishable between control and *Inpp5e*$^{\Delta/\Delta}$;*Gli3*$^{\Delta699/\Delta699}$ embryos (Fig. 7K, Q) and the proportions
337 of Tbr1-Ctip2+ and basal progenitors were not affected any longer (Fig. 7K, L. P-S). Taken together,
338 these findings indicate that re-introducing a single copy of the *Gli3R* allele into the *Inpp5e* mutant
339 background leads to a partial rescue of cortical neurogenesis in *Inpp5e*$^{\Delta/\Delta}$ embryos whereas two
340 copies are required for a full rescue.
341

342 **DISCUSSION**

343 Generating a functional cerebral cortex requires a finely tuned balance between direct and
344 indirect neurogenesis to form subtypes of cortical projection neurons in appropriate numbers. Here,
345 we show that the ciliary mouse mutants *Inpp5e* and *Tctn2* present with a transient increase in
346 neurons forming directly from radial glia progenitors in the lateral neocortex at the expense of basal
347 progenitor formation. This increase in neurogenesis results in augmented formation of Ctip2+ layer
348 V neurons in the *Inpp5e* mutant cortex. Our studies also revealed that the *Inpp5e* mutation interfered
349 with the stability of the RGC primary cilium and its signaling functions, leading to a reduction in the
350 Gli3R levels. Since re-introducing Gli3R in an *Inpp5e* mutant background restored the decreased
351 formation of normal proportions of basal progenitors and neurons, our findings implicate a novel role
352 for primary cilia in controlling the signaling events that direct the decision of RGCs to undergo either
353 direct or indirect neurogenesis.

354

355 **Primary cilia affect the decision between direct and indirect neurogenesis**

356 Radial glial cells in the developing mouse neocortex have the potential to undergo symmetric
357 proliferative or asymmetric cell divisions with the latter division mode producing neurons in a direct
358 manner or indirectly via basal progenitors. Balancing out these division modes is important not only
359 to determine final neuronal output and cortical size but also the types of cortical projection neurons
360 and, hence, subtype composition of the adult neocortex. In the E12.5 *Inpp5e* and *Tctn2* mouse
361 mutants, we identified an increased formation of neurons in the lateral neocortex. Based on our cell
362 cycle exit experiment additional neurons are formed from RGCs at the expense of basal progenitors.
363 Given the cell cycle length of basal progenitors of >24 hours (Arai et al., 2011), it is unlikely that new
364 born basal progenitors would have undergone an additional round of cell division to produce two
365 neurons within the time frame of this experiment. Such an extra division would also have diluted the
366 BrdU label. We therefore conclude that the *Inpp5e* mutation caused RGCs to preferentially produce
367 neurons directly.

368 Interestingly, this increase in direct neurogenesis led to an increased proportion of Ctip2+
369 deep layer V neurons in the E18.5 neocortex but did not coincide with a reduced proportion of upper
370 layer neurons. This effect could be explained in several mutually non-exclusive ways. First, neurons
371 born at E12.5 initially express both Ctip2 and Tbr1 (Fig. 7) and later down-regulate Ctip2. *Inpp5e*
372 could therefore affect the signaling that controls this downregulation. Secondly, the proportions of
373 basal progenitors and neurons was normalized in E14.5 mutants. Since basal progenitors are a main
374 source of upper layer neurons (Arnold et al., 2008; Vasistha et al., 2015), this normalization would
375 account for the sufficient numbers of Satb2+ upper layer neurons. Newly formed projection neurons
376 signal back to RGCS via Jag1, Fgf9 and Neurotrophin 3 (Parthasarathy et al., 2014; Seuntjens et
377 al., 2009; W. Wang et al., 2016) to control the sequential production of deep and upper layer neurons
378 and of glia (Silva et al., 2019). *Inpp5e* might affect these signals by controlling cilia stability and/or
379 levels of $PI(3,4,5)P_3$ (Bielas et al., 2009; Jacoby et al., 2009) that acts as a second messenger in

380 receptor tyrosine kinase signaling. This possibility is supported by our observation that the extent of
381 the pErk expression domain in the neocortex is diminished in E14.5 *Inpp5e*$^{\Delta/\Delta}$ embryos. Regardless
382 of the exact mechanism, our findings suggest a novel, spatially and temporally restricted role for
383 *Inpp5e* in controlling the decision between direct and indirect neurogenesis. This function differs from
384 those described for other cilia mutants. Conditional inactivation of *Ift88* and *Kif3a* leads to a larger
385 cortex (Foerster et al., 2017; Wilson et al., 2012) with a modest increase in BP production in the
386 absence of a delay in neurogenesis (Foerster et al., 2017) while *Rpgrip1l* mutants have reduced
387 numbers of both basal progenitors and neurons (Postel, Karam, Pezeron, Schneider-Maunoury, &
388 Clement, 2019). These findings highlight the multiple and varied roles cilia play in cortical
389 development.
390
391 ***Inpp5e* controls direct/indirect neurogenesis through Gli3 processing**
392 Our study also shed lights into the mechanisms by which *Inpp5e* controls the decision
393 between direct/indirect neurogenesis. Most notably, the Gli3R level and Gli3R/Gli3FL ratio are
394 decreased in *Inpp5e*$^{\Delta/\Delta}$ embryos. While the *Inpp5e* mutation does not lead to an up-regulation of Shh
395 signaling in the dorsal telencephalon (Magnani et al., 2015), re-introducing a single or two copies of
396 Gli3R in an *Inpp5e* mutant background partially and fully restores the neurogenesis defects,
397 respectively. This rescue indicates that reduced levels of Gli3R rather than the reduction in the
398 Gli3R/Gli3FL ratio are responsible for the prevalence of direct neurogenesis in *Inpp5e*$^{\Delta/\Delta}$ embryos.
399 This idea is consistent with the findings that (i) *Gli3*$^{\Delta699/\Delta699}$ embryos that cannot produce Gli3FL and
400 Gli3A show no obvious phenotype in cortical development (Besse et al., 2011; Böse et al., 2002),
401 (ii) dorsal telencephalic patterning defects in *Gli3*$^{Xt/Xt}$ mutants are not rescued in *Shh*$^{-/-}$/*Gli3*^{XtXt} double
402 mutants (Rallu et al., 2002; Rash & Grove, 2007), (iii) Shh promotes the generation of olfactory bulb
403 interneurons and cortical oligodendrocytes and neurogenesis in the subventricular zone by reducing
404 Gli3R rather than by promoting Gli activator function (Petrova, Garcia, & Joyner, 2013; H. Wang,
405 Kane, Lee, & Ahn, 2014; Zhang et al., 2020). In addition, there is also a dramatic rescue of eye
406 development and the rescue also extends to other malformations of the *Inpp5e*$^{\Delta/\Delta}$ forebrain, including
407 the corpus callosum, the hippocampus and the expansion of the piriform cortex, structures that are
408 also affected in *Gli3* null and hypomorphic mutants (Amaniti et al., 2015; Johnson, 1967; Magnani
409 et al., 2014; Theil, Alvarez-Bolado, Walter, & Rüther, 1999; Wiegering, Petzsch, Kohrer, Ruther, &
410 Gerhardt, 2019). Taken together, these findings support the idea that *Inpp5e* and the primary cilium
411 control key processes in cortical development by regulating the formation of Gli3R.
412 Our analyses support several mutually non-exclusive mechanisms how the *Inpp5e* mutation
413 impacts on Gli3 processing. First, our electron microscopy study revealed severe structural
414 abnormalities in large proportions of cilia. The Inpp5e phosphatase hydrolyses PI(3,4,5)P_3, which is
415 essential for the effective activation of the serine threonine kinase Akt (Kisseleva et al., 2002;
416 Plotnikova et al., 2015). Following PIP3 binding, Akt translocates to the membrane and becomes
417 phosphorylated at T308 by phosphoinositide dependent kinase-1 (Pdk1) and at S473 by mammalian

418 target of rapamycin complex (mTORC2) (Yu & Cui, 2016). Consistent with the loss of *Inpp5e* function
419 and a resulting increase in PI(3,4,5)P_3, our western blot analysis revealed elevated pAkt^{S473} levels.
420 Increased phosphorylation at this site has been implicated in inhibiting cilia assembly and promoting
421 cilia disassembly (Mao et al., 2019) and could hence explain the structural defects of RGC *Inpp5e*$^{\Delta/\Delta}$
422 cilia. Secondly, *Inpp5e* could control Gli3 processing through its effect on the transition zone (TZ). It
423 is required for TZ molecular organisation (Dyson et al., 2017) and its substrate PI(4,5)P2 plays a
424 role in TZ maturation in Drosophila (Gupta, Fabian, & Brill, 2018). This model is further supported by
425 our finding that a mouse mutant for the TZ protein Tctn2 phenocopies the *Inpp5e*$^{\Delta/\Delta}$ neurogenesis
426 defect. In turn, several mouse mutants defective for TZ proteins show microphthalmia (Garcia-
427 Gonzalo et al., 2011; Sang et al., 2011; Yee et al., 2015). Tctn proteins are also required for Gli3
428 processing (Sang et al., 2011; Thomas et al., 2012; C. Wang, Li, Meng, & Wang, 2017) and the TZ
429 protein Rpgrip1l controls the activity of the proteasome at the basal body responsible for proteolytic
430 cleavage of Gli3 (Gerhardt et al., 2015). Taken together, these findings indicate that *Inpp5e* mutation
431 might affect the ability of RGCs to switch to indirect neurogenesis through defects in cilia stability
432 and/or the integrity of the ciliary transition zone.
433
434 **Implications for Joubert Syndrome**
435 In humans, hypomorphic *INPP5E* mutations contribute to Joubert Syndrome (JS), a
436 ciliopathy characterized by cerebellar malformations and concomitant ataxia and breathing
437 abnormalities. In addition, a subset of JS patients exhibit cortical abnormalities including
438 polymicrogyria, neuronal heterotopias and agenesis of the corpus callosum (Poretti, Huisman,
439 Scheer, & Boltshauser, 2011). Strikingly, the *Inpp5e* mouse mutant also shows several of these
440 abnormalities. In the caudal telencephalon, the otherwise lissencephalic cortex formed folds
441 reminiscent of the polymicrogyria in JS patients. In addition, the mutant formed leptomeningeal
442 heterotopias with 100% penetrance, but their number and location varied. Mutations in ciliary genes
443 were previously associated with heterotopia formation in humans and mice (Magnani et al., 2015;
444 Uzquiano et al., 2019). Mice carrying mutations in the *Eml1* gene encoding a microtubule-associated
445 protein show subcortical heterotopias due to a mispositioning of radial glial cells and impaired
446 primary cilia formation (Uzquiano et al., 2019). Finally, the corpus callosum is thinner but callosal
447 axons normally project to the contralateral cerebral hemisphere in *Inpp5e* mutants. This phenotype
448 is milder compared to that of other mouse mutants with altered cilia that show complete agenesis of
449 the corpus callosum with callosal axons forming Probst bundles (Benadiba et al., 2012; Laclef et al.,
450 2015; Putoux et al., 2019). Unlike these other ciliary mutants, the corticoseptal boundary which plays
451 a crucial role in positioning guidepost cells that control midline crossing of callosal axons (Magnani
452 et al., 2014) is not obviously affected in *Inpp5e*$^{\Delta/\Delta}$ embryos. Instead, the thinner corpus callosum is
453 likely to be the result of an expanded piriform cortex. Despite these mechanistic differences,
454 however, re-introducing Gli3R into the cilia mutant background restores callosal development in both
455 groups of mutants suggesting that cilia control two independent steps in corpus callosum formation

456 by regulating Gli3 processing. Thus, the *Inpp5e*$^{\Delta/\Delta}$ mutant recapitulates cortical abnormalities in JS
457 patients and starts to help unravelling the pathomechanisms underlying these defects.
458

459 **MATERIAL & METHODS**

460

461 **Mice**

462 All experimental work was carried out in accordance with the UK Animals (Scientific Procedures) Act
463 1986 and UK Home Office guidelines. All protocols were reviewed and approved by the named
464 veterinary surgeons of the College of Medicine and Veterinary Medicine, the University of Edinburgh,
465 prior to the commencement of experimental work. *Inpp5e*$^{\Delta/+}$ and *Gli3*$^{\Delta699/+}$ mouse lines have been
466 described previously (Böse et al., 2002; Jacoby et al., 2009). *Inpp5e*$^{\Delta/+}$ mice were interbred to
467 generate *Inpp5e*$^{\Delta/\Delta}$ embryos; exencephalic *Inpp5e*$^{\Delta/\Delta}$ embryos were excluded from the analyses.
468 Wild-type and *Inpp5e*$^{\Delta/+}$ litter mate embryos served as controls. *Inpp5e*$^{\Delta/\Delta}$;*Gli3*$^{\Delta699/+}$ and
469 *Inpp5e*$^{\Delta/\Delta}$;*Gli3*$^{\Delta699/\Delta699}$ embryos were obtained from inter-crosses of *Inpp5e*$^{\Delta/+}$;*Gli3*$^{\Delta699/+}$ mice using
470 wild-type, *Inpp5e*$^{\Delta/+}$ and *Gli3*$^{\Delta699/+}$ embryos as controls. Embryonic (E) day 0.5 was assumed to start
471 at midday of the day of vaginal plug discovery. Transgenic animals and embryos were genotyped as
472 described (Böse et al., 2002; Jacoby et al., 2009). For each marker and each stage, 3-8 embryos
473 were analysed.

474 For measuring cell cycle lengths, pregnant females were intraperitoneally injected with a
475 single dose of IdU (10mg/ml) at E12.5, followed by an injection of BrdU (10mg/ml) 90 min later.
476 Embryos were harvested 30 min after the second injection. For cell cycle exit analyses, BrdU was
477 injected peritoneally into E11.5 pregnant females and embryos were harvested 24 hrs later.
478 Rapamycin was dissolved in 100% EtOH and diluted in vehicle containing 5% PEG400, 5% Tween80
479 immediately before use. E11.5 pregnant females received a single intraperitoneal injection of
480 Rapamycin at 1 mg/kg body weight or of vehicle and were killed 24 hrs later.

481

482 **Immunohistochemistry and in situ hybridisation**

483 For immunohistochemistry, embryos were fixed overnight in 4% paraformaldehyde, incubated in
484 30% sucrose at +4°C for 24h, embedded in 30% sucrose/OCT mixture (1:1) and frozen on dry ice.
485 Immunofluorescence staining was performed on 12 to 14 μm cryostat sections as described
486 previously (Theil, 2005) with antibodies against Arl13b (Neuromab 75-287; 1:1500), rabbit anti-BrdU
487 (1:50, Abcam #ab6326), mouse anti-BrdU/IdU (B44) (1:50, BD Biosciences #347580), rat anti-Ctip2
488 (1:1000, Abcam #18465), rabbit anti-pErk$^{T202/Y204}$ (1:1000, Cell Signaling Technology #9101), rabbit
489 anti-GFAP (1:1000, Dako #Z 0334), rat anti-L1, clone 324 (1:1000, Millipore #MAB5272), rabbit anti-
490 Pax6 (1:400, Biolegend #901301), mouse anti-PCNA (1:500, Abcam #29), rabbit anti-Prox1 (1:1000,
491 RELIA*Tech* #102-PA32). rabbit anti-pHH3 (1:100, Millipore #06-570), mouse anti-Satb2 (1:200,
492 Abcam #51502), rabbit anti-Tbr1 (1:400, Abcam #31940), rabbit anti-Tbr2 (1:1000, Abcam #23345)
493 and γTUB (Sigma T6557; 1:2000). Primary antibodies for immunohistochemistry were detected with
494 Alexa- or Cy2/3-conjugated fluorescent secondary antibodies. The Tbr1 signals were amplified using
495 biotinylated secondary IgG antibody (swine anti-rabbit IgG) (1:400, BD Biosciences) followed by

496 Alexa Fluor 488 or 568 Streptavidin (1:100, Invitrogen). For counter staining DAPI (1:2000, Life
497 Technologies) was used. Prox1 and pErk$^{T202/Y204}$ proteins were detected non-fluorescently using
498 biotinylated goat anti-rabbit IgG (1: 400, BD Biosciences) followed by avidin-HRP and DAB detection
499 (Vector labs) as described previously (Magnani et al., 2010).
500 In situ hybridisation on 12μm serial paraffin sections were performed as described previously (Theil,
501 2005) using antisense RNA probes for *Axin2* (Lustig et al., 2002), *Bmp4* (Jones, Lyons, & Hogan,
502 1991), *Dbx1* (Yun, Potter, & Rubenstein, 2001), *Dlx2* (Bulfone et al., 1993), *Emx1* (Simeone et al.,
503 1992), *Gli3* (Hui, Slusarski, Platt, Holmgren, & Joyner, 1994), *Lhx2* (Liem, Tremml, & Jessell, 1997),
504 *Msx1 (Hill et al., 1989)*, *Ngn2* (Gradwohl, Fode, & Guillemot, 1996), *Nrp2* (Galceran et al., 2000),
505 *Pax6* (Walther & Gruss, 1991), *Scip1* (Frantz et al., 1994), *Wnt2b* (Grove, Tole, Limon, Yip, &
506 Ragsdale, 1998).
507
508 **Western blot**
509 Protein was extracted from the dorsal telencephalon of E12.5 (3 tissues pooled per sample) and
510 E14.5 (single tissue per sample) wild-type and *Inpp5e*$^{\Delta/\Delta}$ embryos (n=4 samples per genotype) as
511 described previously (Magnani et al., 2010). For the detection of Gli3 10µg protein lysates were
512 subjected to gel electrophoresis on a 3-8% NuPAGE® Tris-Acetate gel (Life Technologies), and
513 protein was transferred to a Immobilon-FL membrane (Millipore), which was incubated with goat
514 anti-h/m Gli3 (1:500, R&D Systems #AF3690) and mouse anti-β-Actin antibody (1:15000, Abcam
515 #ab6276). After incubating with donkey anti-goat IgG IRDye680RD (1:15000, LI-COR Biosciences)
516 and donkey anti-mouse IgG IRDye800CW secondary antibodies (1:15000, Life Technologies),
517 signal was detected using LI-COR's Odyssey Infrared Imaging System with Odyssey Software.
518 Values for protein signal intensity were obtained using Image Studio Lite Version3.1. Gli3 repressor
519 and activator protein levels were compared between wild-type and mutant tissue using a paired t-
520 test.
521 For all other Western blot analyses 20µg protein lysates were loaded on 4–12% NuPAGE® Bis-Tris
522 gels (Life Technologies) and later transferred to an Immobilon–FL membrane. Membranes were
523 incubated with the following primary antibodies: rabbit anti-phospho-Akt^{S473} (1:1000, Cell Signaling
524 Technologies CST #9271), rabbit anti-Akt (1:1000, CST #9272), rabbit anti-phospho-Erk$^{T202/Y204}$
525 (1:1000, CST #9101), rabbit anti-Erk (L34F12) (CST # 4696), rabbit anti-ribosomal protein phospho-
526 S6$^{S235/S236}$ (1:1000, CST #2211), rabbit anti-ribosomal protein phospho-S6$^{S240/S244}$ (1:1000, CST
527 #2215) and mouse anti-ribosomal protein S6 (C-8) (1:1000, Santa Cruz Technologies #sc-74459).
528 For the detection of phosphorylated proteins goat anti-rabbit IRDye 680RD (1:15,000, LI-COR
529 Biosciences) and for total proteins goat anti-mouse or goat anti-rabbit IRDye 800CW (1:15,000, LI-
530 COR Biosciences) were used as secondary antibodies. The signals were detected via the Odyssey
531 Imaging System and further analysed using Image Studio Lite Version4.0. The ratios between
532 phosphorylated and total protein were compated between wild-type and mutant tissue using a paired
533 t-test.

534

535 **Scanning and transmission electron microscopy**

536 TEM and SEM image acquisition were performed in the Cochin Imaging Facility and on the IBPS
537 EM Facility, respectively. For scanning electron microscopy, embryos were dissected in 1.22x PBS
538 (pH 7.4) and fixed overnight with 2% glutaraldehyde in 0.61x PBS (pH 7.4) at 4°C. Heads were then
539 sectioned to separate the dorsal and ventral parts of the telencephalon, exposing their ventricular
540 surfaces. Head samples were washed several times in 1.22x PBS and postfixed for 15 minutes in
541 1.22x PBS containing 1% OsO4. Fixed samples were washed several times in ultrapure water,
542 dehydrated with a graded series of ethanol and prepared for scanning electron microscopy using the
543 critical point procedure (CPD7501, Polaron). Their surfaces were coated with a 20 nm gold layer
544 using a gold spattering device (Scancoat Six, Edwards). Samples were observed under a Cambridge
545 S260 scanning electron microscope at 10 keV.

546 For transmission electron microscopy tissues were fixed for 1 hour with 3% glutaraldehyde, post-
547 fixed in 1.22x PBS containing 1% OsO4, then dehydrated with a graded ethanol series. After 10
548 minutes in a 1:2 mixture of propane:epoxy resin, tissues were embedded in gelatin capsules with
549 freshly prepared epoxy resin and polymerized at 60°C for 24 hours. Sections (80 nm) obtained using
550 an ultramicrotome (Reichert Ultracut S) were stained with uranyl acetate and Reynold's lead citrate
551 and observed with a Philips CM10 transmission electron microscope.

552

553 **Statistical Analyses**

554 Data were analysed using GraphPadPrism 6 software with n=3-8 embryos for all analyses. Power
555 analysis of pilot experiments informed minimum samples size. Mann Whitney tests were performed
556 for immunohistochemical analyses in general. Cortical thickness was analysed using a two way
557 ANOVA followed by Sidak's multiple comparisons test. Paired t-tests were performed for Western
558 blots and a fisher's exact test was used to analyse the quantification of normal and abnormal cilia.
559 The mTORC1 and Gli3 rescue experiments were evaluated with one way ANOVAS followed by
560 Tukey's multiple comparisons test. A single asterisk indicates significance of $p<0.05$, two asterisks
561 indicate significance of $p<0.01$ and three asterisks of $p<0.005$. Due to morphological changes
562 blinding was not possible and scores were validated by a second independent observer.

563

564

565 **ACKNOWLEDGEMENTS**

566

567 We are grateful to Drs Thomas Becker, John Mason, Pleasantine Mill, and David Price for critical
568 comments on the manuscript, Dr Christos Gkogkas for invaluable advice on mTOR signaling, and
569 Stéphane Schurmans for the *Inpp5e*$^{\Delta/+}$ mouse line. We also thank Dr Michaël Trichet (electron
570 microscopy platform of the IBPS-Sorbonne Universités Paris 6) and Dr Alain Schmitt (electron

571 microscopy platform of the Institut Cochin CNRS-UMR 8104) for their help with scanning and
572 transmission electron microscopy analyses, respectively. This work was supported by a grant from
573 the Biotechnology and Biological Sciences Research Council to TT (BB/P00122X/1) and NIH
574 R01GM095941 to JFR.

575

576 **COMPETING INTERESTS**

577

578 The authors declare no competing interests.

579

580

581

582 **REFERENCES**

583

584 Amaniti, E. M., Fu, C., Lewis, S., Saisana, M., Magnani, D., Mason, J. O., & Theil, T. (2015).
585 Expansion of the piriform cortex contributes to corticothalamic pathfinding defects in Gli3
586 conditional mutants. *Cereb Cortex, 25*(2), 460-471. doi:10.1093/cercor/bht244
587 Arai, Y., Pulvers, J. N., Haffner, C., Schilling, B., Nusslein, I., Calegari, F., & Huttner, W. B. (2011).
588 Neural stem and progenitor cells shorten S-phase on commitment to neuron production.
589 *Nature communications, 2*, 154. doi:10.1038/ncomms1155
590 Ariens-Kapers, C. U., Huber, G. C., & Crosby, E. C. (1936). The comparative anatomy of the
591 nervous system of the vertebrates including man. *New York Macmillan*.
592 Arnold, S. J., Huang, G. J., Cheung, A. F., Era, T., Nishikawa, S., Bikoff, E. K., . . . Groszer, M.
593 (2008). The T-box transcription factor Eomes/Tbr2 regulates neurogenesis in the cortical
594 subventricular zone. *Genes Dev, 22*(18), 2479-2484. doi:10.1101/gad.475408
595 Ashique, A. M., Choe, Y., Karlen, M., May, S. R., Phamluong, K., Solloway, M. J., . . . Peterson, A.
596 S. (2009). The Rfx4 transcription factor modulates Shh signaling by regional control of
597 ciliogenesis. *Sci Signal, 2*(95), ra70. doi:10.1126/scisignal.2000602
598 Benadiba, C., Magnani, D., Niquille, M., Morle, L., Valloton, D., Nawabi, H., . . . Durand, B. (2012).
599 The ciliogenic transcription factor RFX3 regulates early midline distribution of guidepost
600 neurons required for corpus callosum development. *PLoS genetics, 8*(3), e1002606.
601 doi:10.1371/journal.pgen.1002606
602 Besse, L., Neti, M., Anselme, I., Gerhardt, C., Ruther, U., Laclef, C., & Schneider-Maunoury, S.
603 (2011). Primary cilia control telencephalic patterning and morphogenesis via Gli3
604 proteolytic processing. *Development, 138*(10), 2079-2088. doi:10.1242/dev.059808
605 Bielas, S. L., Silhavy, J. L., Brancati, F., Kisseleva, M. V., Al-Gazali, L., Sztriha, L., . . . Gleeson, J.
606 G. (2009). Mutations in INPP5E, encoding inositol polyphosphate-5-phosphatase E, link
607 phosphatidyl inositol signaling to the ciliopathies. *Nat Genet, 41*(9), 1032-1036.
608 doi:10.1038/ng.423
609 Böse, J., Grotewold, L., & Rüther, U. (2002). Pallister-Hall syndrome phenotype in mice mutant for
610 Gli3. *Hum Mol Genet, 11*(9), 1129-1135.
611 Bulfone, A., Puelles, L., Porteus, M. H., Frohman, M. A., Martin, G. R., & Rubenstein, J. L. (1993).
612 Spatially restricted expression of Dlx-1, Dlx-2 (Tes-1), Gbx-2, and Wnt-3 in the embryonic
613 day 12.5 mouse forebrain defines potential transverse and longitudinal segmental
614 boundaries. *J Neurosci, 13*(7), 3155-3172.
615 Cardenas, A., Villalba, A., de Juan Romero, C., Pico, E., Kyrousi, C., Tzika, A. C., . . . Borrell, V.
616 (2018). Evolution of Cortical Neurogenesis in Amniotes Controlled by Robo Signaling
617 Levels. *Cell, 174*(3), 590-606 e521. doi:10.1016/j.cell.2018.06.007
618 Caspary, T., Larkins, C. E., & Anderson, K. V. (2007). The graded response to Sonic Hedgehog
619 depends on cilia architecture. *Developmental cell, 12*(5), 767-778.
620 doi:10.1016/j.devcel.2007.03.004
621 Chavez, M., Ena, S., Van Sande, J., de Kerchove d'Exaerde, A., Schurmans, S., & Schiffmann, S.
622 N. (2015). Modulation of Ciliary Phosphoinositide Content Regulates Trafficking and Sonic
623 Hedgehog Signaling Output. *Developmental cell, 34*(3), 338-350.
624 doi:10.1016/j.devcel.2015.06.016
625 Dyson, J. M., Conduit, S. E., Feeney, S. J., Hakim, S., DiTommaso, T., Fulcher, A. J., . . . Mitchell,
626 C. A. (2017). INPP5E regulates phosphoinositide-dependent cilia transition zone function. *J*
627 *Cell Biol, 216*(1), 247-263. doi:10.1083/jcb.201511055
628 Englund, C., Fink, A., Lau, C., Pham, D., Daza, R. A., Bulfone, A., . . . Hevner, R. F. (2005). Pax6,
629 Tbr2, and Tbr1 are expressed sequentially by radial glia, intermediate progenitor cells, and
630 postmitotic neurons in developing neocortex. *J Neurosci, 25*(1), 247-251.
631 Ferrari, S., Bandi, H. R., Hofsteenge, J., Bussian, B. M., & Thomas, G. (1991). Mitogen-activated
632 70K S6 kinase. Identification of in vitro 40 S ribosomal S6 phosphorylation sites. *J Biol*
633 *Chem, 266*(33), 22770-22775.
634 Florio, M., & Huttner, W. B. (2014). Neural progenitors, neurogenesis and the evolution of the
635 neocortex. *Development, 141*(11), 2182-2194. doi:10.1242/dev.090571

636 Foerster, P., Daclin, M., Asm, S., Faucourt, M., Boletta, A., Genovesio, A., & Spassky, N. (2017).
637 mTORC1 signaling and primary cilia are required for brain ventricle morphogenesis.
638 *Development, 144*(2), 201-210. doi:10.1242/dev.138271
639 Fotaki, V., Yu, T., Zaki, P. A., Mason, J. O., & Price, D. J. (2006). Abnormal positioning of
640 diencephalic cell types in neocortical tissue in the dorsal telencephalon of mice lacking
641 functional Gli3. *J Neurosci, 26*(36), 9282-9292.
642 Frantz, G. D., Bohner, A. P., Akers, R. M., & McConnell, S. K. (1994). Regulation of the POU
643 domain gene SCIP during cerebral cortical development. *J Neurosci, 14*(2), 472-485.
644 Galceran, J., Miyashita-Lin, E. M., Devaney, E., Rubenstein, J. L., & Grosschedl, R. (2000).
645 Hippocampus development and generation of dentate gyrus granule cells is regulated by
646 LEF1. *Development, 127*(3), 469-482.
647 Garcia-Gonzalo, F. R., Corbit, K. C., Sirerol-Piquer, M. S., Ramaswami, G., Otto, E. A., Noriega, T.
648 R., . . . Reiter, J. F. (2011). A transition zone complex regulates mammalian ciliogenesis
649 and ciliary membrane composition. *Nat Genet, 43*(8), 776-784. doi:10.1038/ng.891
650 Garcia-Gonzalo, F. R., Phua, S. C., Roberson, E. C., Garcia, G., 3rd, Abedin, M., Schurmans, S., .
651 . . Reiter, J. F. (2015). Phosphoinositides Regulate Ciliary Protein Trafficking to Modulate
652 Hedgehog Signaling. *Developmental cell, 34*(4), 400-409. doi:10.1016/j.devcel.2015.08.001
653 Gerhardt, C., Lier, J. M., Burmuhl, S., Struchtrup, A., Deutschmann, K., Vetter, M., . . . Ruther, U.
654 (2015). The transition zone protein Rpgrip1l regulates proteasomal activity at the primary
655 cilium. *J Cell Biol, 210*(1), 115-133. doi:10.1083/jcb.201408060
656 Gladwyn-Ng, I., Cordon-Barris, L., Alfano, C., Creppe, C., Couderc, T., Morelli, G., . . . Nguyen, L.
657 (2018). Stress-induced unfolded protein response contributes to Zika virus-associated
658 microcephaly. *Nature neuroscience, 21*(1), 63-71. doi:10.1038/s41593-017-0038-4
659 Götz, M., Stoykova, A., & Gruss, P. (1998). Pax6 controls radial glia differentiation in the cerebral
660 cortex. *Neuron, 21*(5), 1031-1044.
661 Gradwohl, G., Fode, C., & Guillemot, F. (1996). Restricted expression of a novel murine atonal-
662 related bHLH protein in undifferentiated neural precursors. *Dev Biol, 180*(1), 227-241.
663 Grove, E. A., Tole, S., Limon, J., Yip, L., & Ragsdale, C. W. (1998). The hem of the embryonic
664 cerebral cortex is defined by the expression of multiple Wnt genes and is compromised in
665 Gli3-deficient mice. *Development, 125*(12), 2315-2325.
666 Gupta, A., Fabian, L., & Brill, J. A. (2018). Phosphatidylinositol 4,5-bisphosphate regulates cilium
667 transition zone maturation in Drosophila melanogaster. *J Cell Sci, 131*(16).
668 doi:10.1242/jcs.218297
669 Hall, P. A., Levison, D. A., Woods, A. L., Yu, C. C., Kellock, D. B., Watkins, J. A., . . . et al. (1990).
670 Proliferating cell nuclear antigen (PCNA) immunolocalization in paraffin sections: an index
671 of cell proliferation with evidence of deregulated expression in some neoplasms. *J Pathol,*
672 *162*(4), 285-294. doi:10.1002/path.1711620403
673 Hasenpusch-Theil, K., West, S., Kelman, A., Kozic, Z., Horrocks, S., McMahon, A. P., . . . Theil, T.
674 (2018). Gli3 controls the onset of cortical neurogenesis by regulating the radial glial cell
675 cycle through Cdk6 expression. *Development, 145*(17). doi:10.1242/dev.163147
676 Haubensak, W., Attardo, A., Denk, W., & Huttner, W. B. (2004). Neurons arise in the basal
677 neuroepithelium of the early mammalian telencephalon: a major site of neurogenesis. *Proc*
678 *Natl Acad Sci U S A, 101*(9), 3196-3201.
679 Hill, R. E., Jones, P. F., Rees, A. R., Sime, C. M., Justice, M. J., Copeland, N. G., . . . Davidson, D.
680 R. (1989). A new family of mouse homeo box-containing genes: molecular structure,
681 chromosomal location, and developmental expression of Hox-7.1. *Genes Dev, 3*(1), 26-37.
682 Hui, C. C., Slusarski, D., Platt, K. A., Holmgren, R., & Joyner, A. L. (1994). Expression of three
683 mouse homologs of the Drosophila segment polarity gene cubitus interruptus, Gli, Gli-2,
684 and Gli-3, in ectoderm- and mesoderm-derived tissues suggests multiple roles during
685 postimplantation development. *Dev Biol, 162*(2), 402-413.
686 Jacoby, M., Cox, J. J., Gayral, S., Hampshire, D. J., Ayub, M., Blockmans, M., . . . Schurmans, S.
687 (2009). INPP5E mutations cause primary cilium signaling defects, ciliary instability and
688 ciliopathies in human and mouse. *Nat Genet, 41*(9), 1027-1031.
689 Johnson, D. R. (1967). Extra-toes: a new mutant gene causing multiple abnormalities in the
690 mouse. *J Embryol Exp Morphol, 17*(3), 543-581.

691 Jones, C. M., Lyons, K. M., & Hogan, B. L. (1991). Involvement of Bone Morphogenetic Protein-4
692 (BMP-4) and Vgr-1 in morphogenesis and neurogenesis in the mouse. *Development,*
693 *111*(2), 531-542.
694 Kisseleva, M. V., Cao, L., & Majerus, P. W. (2002). Phosphoinositide-specific inositol
695 polyphosphate 5-phosphatase IV inhibits Akt/protein kinase B phosphorylation and leads to
696 apoptotic cell death. *J Biol Chem, 277*(8), 6266-6272. doi:10.1074/jbc.M105969200
697 Laclef, C., Anselme, I., Besse, L., Catala, M., Palmyre, A., Baas, D., . . . Schneider-Maunoury, S.
698 (2015). The role of primary cilia in corpus callosum formation is mediated by production of
699 the Gli3 repressor. *Hum Mol Genet, 24*(17), 4997-5014. doi:10.1093/hmg/ddv221
700 Laguesse, S., Creppe, C., Nedialkova, D. D., Prevot, P. P., Borgs, L., Huysseune, S., . . . Nguyen,
701 L. (2015). A Dynamic Unfolded Protein Response Contributes to the Control of Cortical
702 Neurogenesis. *Developmental cell, 35*(5), 553-567. doi:10.1016/j.devcel.2015.11.005
703 Lee, S. M., Tole, S., Grove, E., & McMahon, A. P. (2000). A local Wnt-3a signal is required for
704 development of the mammalian hippocampus. *Development, 127*(3), 457-467.
705 Liem, K. F., Jr., Tremml, G., & Jessell, T. M. (1997). A role for the roof plate and its resident
706 TGFbeta-related proteins in neuronal patterning in the dorsal spinal cord. *Cell, 91*(1), 127-
707 138.
708 Lustig, B., Jerchow, B., Sachs, M., Weiler, S., Pietsch, T., Karsten, U., . . . Behrens, J. (2002).
709 Negative Feedback Loop of Wnt Signaling through Upregulation of Conductin/Axin2 in
710 Colorectal and Liver Tumors. *Mol. Cell. Biol., 22*(4), 1184-1193.
711 Magnani, D., Hasenpusch-Theil, K., Benadiba, C., Yu, T., Basson, M. A., Price, D. J., . . . Theil, T.
712 (2014). Gli3 controls corpus callosum formation by positioning midline guideposts during
713 telencephalic patterning. *Cerebral cortex, 24*(1), 186-198. doi:10.1093/cercor/bhs303
714 Magnani, D., Hasenpusch-Theil, K., Jacobs, E. C., Campagnoni, A. T., Price, D. J., & Theil, T.
715 (2010). The Gli3 hypomorphic mutation Pdn causes selective impairment in the growth,
716 patterning, and axon guidance capability of the lateral ganglionic eminence. *J Neurosci,*
717 *30*(41), 13883-13894. doi:30/41/13883 [pii]
718 10.1523/JNEUROSCI.3650-10.2010
719 Magnani, D., Morle, L., Hasenpusch-Theil, K., Paschaki, M., Jacoby, M., Schurmans, S., . . . Theil,
720 T. (2015). The ciliogenic transcription factor Rfx3 is required for the formation of the
721 thalamocortical tract by regulating the patterning of prethalamus and ventral telencephalon.
722 *Hum Mol Genet, 24*(9), 2578-2593. doi:10.1093/hmg/ddv021
723 Mao, H., Tang, Z., Li, H., Sun, B., Tan, M., Fan, S., . . . Sun, Y. (2019). Neddylation inhibitor
724 MLN4924 suppresses cilia formation by modulating AKT1. *Protein Cell*.
725 doi:10.1007/s13238-019-0614-3
726 Martinez-Cerdeno, V., Noctor, S. C., & Kriegstein, A. R. (2006). The role of intermediate progenitor
727 cells in the evolutionary expansion of the cerebral cortex. *Cereb Cortex, 16 Suppl 1*, i152-
728 161. doi:10.1093/cercor/bhk017
729 Martynoga, B., Morrison, H., Price, D. J., & Mason, J. O. (2005). Foxg1 is required for specification
730 of ventral telencephalon and region-specific regulation of dorsal telencephalic precursor
731 proliferation and apoptosis. *Dev Biol, 283*(1), 113-127.
732 Miyata, T., Kawaguchi, A., Saito, K., Kawano, M., Muto, T., & Ogawa, M. (2004). Asymmetric
733 production of surface-dividing and non-surface-dividing cortical progenitor cells.
734 *Development, 131*(13), 3133-3145. doi:10.1242/dev.01173
735 Noctor, S. C., Martinez-Cerdeno, V., Ivic, L., & Kriegstein, A. R. (2004). Cortical neurons arise in
736 symmetric and asymmetric division zones and migrate through specific phases. *Nature*
737 *neuroscience, 7*(2), 136-144. doi:10.1038/nn1172
738 Nowakowski, R. S., Lewin, S. B., & Miller, M. W. (1989). Bromodeoxyuridine immunohistochemical
739 determination of the lengths of the cell cycle and the DNA-synthetic phase for an
740 anatomically defined population. *J Neurocytol, 18*(3), 311-318.
741 Oliver, G., Sosa-Pineda, B., Geisendorf, S., Spana, E. P., Doe, C. Q., & Gruss, P. (1993). Prox 1,
742 a prospero-related homeobox gene expressed during mouse development. *Mech Dev,*
743 *44*(1), 3-16. doi:10.1016/0925-4773(93)90012-m
744 Parthasarathy, S., Srivatsa, S., Nityanandam, A., & Tarabykin, V. (2014). Ntf3 acts downstream of
745 Sip1 in cortical postmitotic neurons to control progenitor cell fate through feedback
746 signaling. *Development, 141*(17), 3324-3330. doi:10.1242/dev.114173

Petrova, R., Garcia, A. D., & Joyner, A. L. (2013). Titration of GLI3 repressor activity by sonic hedgehog signaling is critical for maintaining multiple adult neural stem cell and astrocyte functions. *The Journal of neuroscience : the official journal of the Society for Neuroscience, 33*(44), 17490-17505. doi:10.1523/JNEUROSCI.2042-13.2013

Plotnikova, O. V., Seo, S., Cottle, D. L., Conduit, S., Hakim, S., Dyson, J. M., . . . Smyth, I. M. (2015). INPP5E interacts with AURKA, linking phosphoinositide signaling to primary cilium stability. *J Cell Sci, 128*(2), 364-372. doi:10.1242/jcs.161323

Poretti, A., Huisman, T. A., Scheer, I., & Boltshauser, E. (2011). Joubert syndrome and related disorders: spectrum of neuroimaging findings in 75 patients. *AJNR Am J Neuroradiol, 32*(8), 1459-1463. doi:10.3174/ajnr.A2517

Postel, M., Karam, A., Pezeron, G., Schneider-Maunoury, S., & Clement, F. (2019). A multiscale mathematical model of cell dynamics during neurogenesis in the mouse cerebral cortex. *BMC Bioinformatics, 20*(1), 470. doi:10.1186/s12859-019-3018-8

Postiglione, M. P., Juschke, C., Xie, Y., Haas, G. A., Charalambous, C., & Knoblich, J. A. (2011). Mouse inscuteable induces apical-basal spindle orientation to facilitate intermediate progenitor generation in the developing neocortex. *Neuron, 72*(2), 269-284. doi:10.1016/j.neuron.2011.09.022

Putoux, A., Baas, D., Paschaki, M., Morle, L., Maire, C., Attie-Bitach, T., . . . Durand, B. (2019). Altered GLI3 and FGF8 signaling underlies acrocallosal syndrome phenotypes in Kif7 depleted mice. *Hum Mol Genet, 28*(6), 877-887. doi:10.1093/hmg/ddy392

Rallu, M., Machold, R., Gaiano, N., Corbin, J. G., McMahon, A. P., & Fishell, G. (2002). Dorsoventral patterning is established in the telencephalon of mutants lacking both Gli3 and Hedgehog signaling. *Development, 129*(21), 4963-4974.

Rash, B. G., & Grove, E. A. (2007). Patterning the dorsal telencephalon: a role for sonic hedgehog? *J Neurosci, 27*(43), 11595-11603.

Reiter, J. F., & Skarnes, W. C. (2006). Tectonic, a novel regulator of the Hedgehog pathway required for both activation and inhibition. *Genes Dev, 20*(1), 22-27. doi:10.1101/gad.1363606

Sang, L., Miller, J. J., Corbit, K. C., Giles, R. H., Brauer, M. J., Otto, E. A., . . . Jackson, P. K. (2011). Mapping the NPHP-JBTS-MKS protein network reveals ciliopathy disease genes and pathways. *Cell, 145*(4), 513-528. doi:10.1016/j.cell.2011.04.019

Seuntjens, E., Nityanandam, A., Miquelajauregui, A., Debruyn, J., Stryjewska, A., Goebbels, S., . . . Tarabykin, V. (2009). Sip1 regulates sequential fate decisions by feedback signaling from postmitotic neurons to progenitors. *Nature neuroscience, 12*(11), 1373-1380. doi:10.1038/nn.2409

Shi, X., Garcia, G., 3rd, Van De Weghe, J. C., McGorty, R., Pazour, G. J., Doherty, D., . . . Reiter, J. F. (2017). Super-resolution microscopy reveals that disruption of ciliary transition-zone architecture causes Joubert syndrome. *Nat Cell Biol, 19*(10), 1178-1188. doi:10.1038/ncb3599

Silva, C. G., Peyre, E., & Nguyen, L. (2019). Cell migration promotes dynamic cellular interactions to control cerebral cortex morphogenesis. *Nat Rev Neurosci, 20*(6), 318-329. doi:10.1038/s41583-019-0148-y

Simeone, A., Gulisano, M., Acampora, D., Stornaiuolo, A., Rambaldi, M., & Boncinelli, E. (1992). Two vertebrate homeobox genes related to the Drosophila empty spiracles gene are expressed in the embryonic cerebral cortex. *EMBO J, 11*(7), 2541-2550.

Theil, T. (2005). Gli3 is required for the specification and differentiation of preplate neurons. *Dev Biol, 286*(2), 559-571.

Theil, T., Alvarez-Bolado, G., Walter, A., & Rüther, U. (1999). Gli3 is required for Emx gene expression during dorsal telencephalon development. *Development, 126*(16), 3561-3571.

Thomas, S., Legendre, M., Saunier, S., Bessieres, B., Alby, C., Bonniere, M., . . . Attie-Bitach, T. (2012). TCTN3 mutations cause Mohr-Majewski syndrome. *Am J Hum Genet, 91*(2), 372-378. doi:10.1016/j.ajhg.2012.06.017

Uzquiano, A., Cifuentes-Diaz, C., Jabali, A., Romero, D. M., Houllier, A., Dingli, F., . . . Francis, F. (2019). Mutations in the Heterotopia Gene Eml1/EML1 Severely Disrupt the Formation of Primary Cilia. *Cell Rep, 28*(6), 1596-1611 e1510. doi:10.1016/j.celrep.2019.06.096

Valente, E. M., Rosti, R. O., Gibbs, E., & Gleeson, J. G. (2014). Primary cilia in neurodevelopmental disorders. *Nat Rev Neurol, 10*(1), 27-36. doi:10.1038/nrneurol.2013.247

Vasistha, N. A., Garcia-Moreno, F., Arora, S., Cheung, A. F., Arnold, S. J., Robertson, E. J., & Molnar, Z. (2015). Cortical and Clonal Contribution of Tbr2 Expressing Progenitors in the Developing Mouse Brain. *Cereb Cortex, 25*(10), 3290-3302. doi:10.1093/cercor/bhu125

Walther, C., & Gruss, P. (1991). Pax-6, a murine paired box gene, is expressed in the developing CNS. *Development, 113*(4), 1435-1449.

Wang, C., Li, J., Meng, Q., & Wang, B. (2017). Three Tctn proteins are functionally conserved in the regulation of neural tube patterning and Gli3 processing but not ciliogenesis and Hedgehog signaling in the mouse. *Dev Biol, 430*(1), 156-165. doi:10.1016/j.ydbio.2017.08.003

Wang, H., Ge, G., Uchida, Y., Luu, B., & Ahn, S. (2011). Gli3 is required for maintenance and fate specification of cortical progenitors. *J Neurosci, 31*(17), 6440-6448. doi:31/17/6440 [pii] 10.1523/JNEUROSCI.4892-10.2011

Wang, H., Kane, A. W., Lee, C., & Ahn, S. (2014). Gli3 repressor controls cell fates and cell adhesion for proper establishment of neurogenic niche. *Cell Rep, 8*(4), 1093-1104. doi:10.1016/j.celrep.2014.07.006

Wang, W., Jossin, Y., Chai, G., Lien, W. H., Tissir, F., & Goffinet, A. M. (2016). Feedback regulation of apical progenitor fate by immature neurons through Wnt7-Celsr3-Fzd3 signalling. *Nature communications, 7*, 10936. doi:10.1038/ncomms10936

Warren, N., Caric, D., Pratt, T., Clausen, J. A., Asavaritikrai, P., Mason, J. O., . . . Price, D. J. (1999). The transcription factor, Pax6, is required for cell proliferation and differentiation in the developing cerebral cortex. *Cereb Cortex, 9*(6), 627-635.

Wiegering, A., Petzsch, P., Kohrer, K., Ruther, U., & Gerhardt, C. (2019). GLI3 repressor but not GLI3 activator is essential for mouse eye patterning and morphogenesis. *Dev Biol, 450*(2), 141-154. doi:10.1016/j.ydbio.2019.02.018

Willaredt, M. A., Hasenpusch-Theil, K., Gardner, H. A., Kitanovic, I., Hirschfeld-Warneken, V. C., Gojak, C. P., . . . Tucker, K. L. (2008). A crucial role for primary cilia in cortical morphogenesis. *J Neurosci, 28*(48), 12887-12900.

Wilson, S. L., Wilson, J. P., Wang, C., Wang, B., & McConnell, S. K. (2012). Primary cilia and Gli3 activity regulate cerebral cortical size. *Dev Neurobiol, 72*(9), 1196-1212. doi:10.1002/dneu.20985

Yee, L. E., Garcia-Gonzalo, F. R., Bowie, R. V., Li, C., Kennedy, J. K., Ashrafi, K., . . . Reiter, J. F. (2015). Conserved Genetic Interactions between Ciliopathy Complexes Cooperatively Support Ciliogenesis and Ciliary Signaling. *PLoS Genet, 11*(11), e1005627. doi:10.1371/journal.pgen.1005627

Yu, J. S., & Cui, W. (2016). Proliferation, survival and metabolism: the role of PI3K/AKT/mTOR signalling in pluripotency and cell fate determination. *Development, 143*(17), 3050-3060. doi:10.1242/dev.137075

Yun, K., Potter, S., & Rubenstein, J. L. (2001). Gsh2 and Pax6 play complementary roles in dorsoventral patterning of the mammalian telencephalon. *Development, 128*(2), 193-205.

Zhang, Y., Liu, G., Guo, T., Liang, X. G., Du, H., Yang, L., . . . Chen, B. (2020). Cortical Neural Stem Cell Lineage Progression Is Regulated by Extrinsic Signaling Molecule Sonic Hedgehog. *Cell Rep, 30*(13), 4490-4504 e4494. doi:10.1016/j.celrep.2020.03.027

849 **FIGURES**

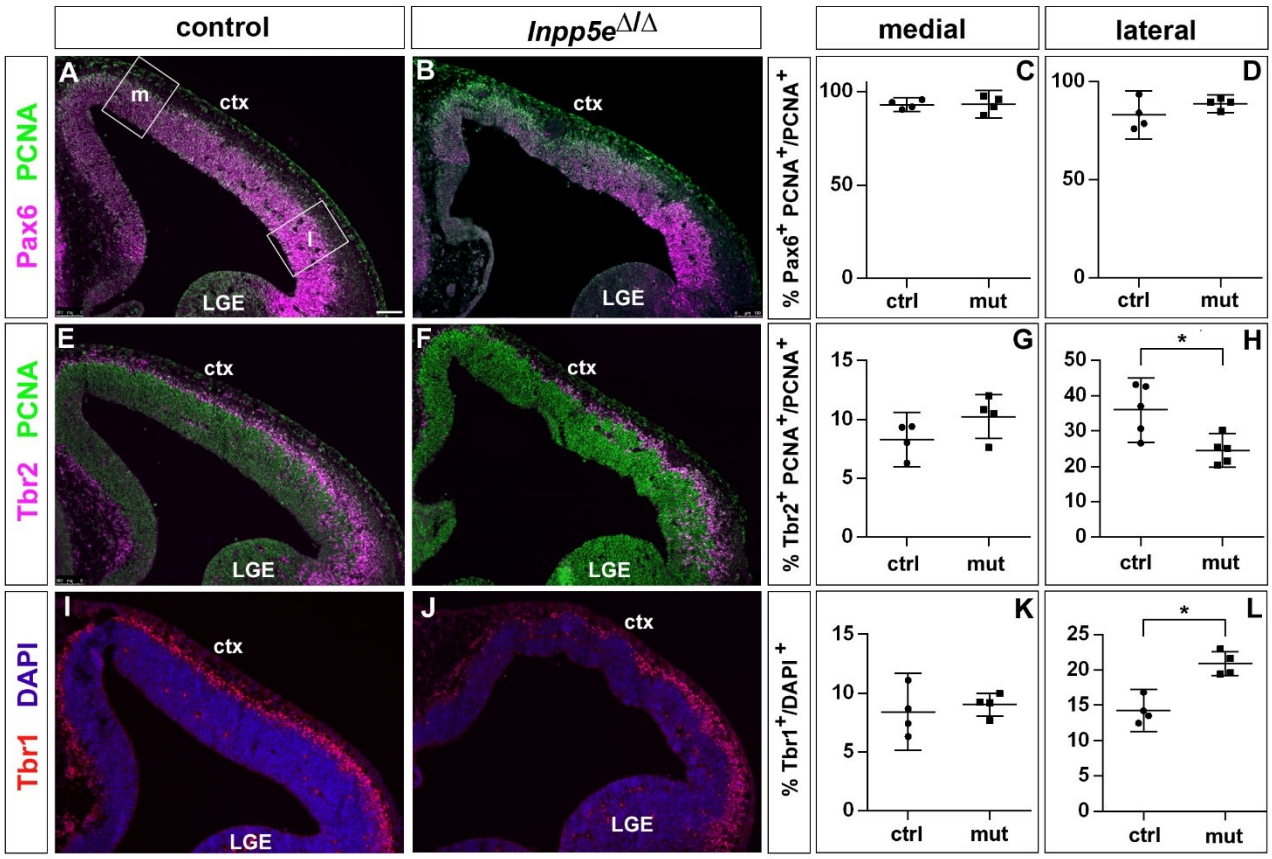

850

851 **Figure 1: Increased neuron formation in the dorsolateral telencephalon of E12.5 *Inpp5*$^{\Delta/\Delta}$**
852 **mutant embryos**. (A-D) Pax6/PCNA double immunofluorescence staining revealed the proportion
853 of apical radial glial cells which remained unaltered in the mutant. The boxes in (A) indicate the
854 regions in the medial (m) and lateral (l) telencephalon at which cell counts were performed. (E-H)
855 Reduced proportions of basal progenitors in the lateral telencephalon as revealed by staining for
856 Tbr2 and PCNA. (I-L) Tbr1 immunostaining showed that the proportion of neurons is increased in
857 the lateral telencephalon. All statistical data are presented as means ± 95% confidence intervals
858 (CI); Mann Whitney tests; n = 4 except for (H) with n=5; * $p < 0.05$. Scale bar: 100μm. ctx: cortex;
859 LGE: lateral ganglionic eminence.

860

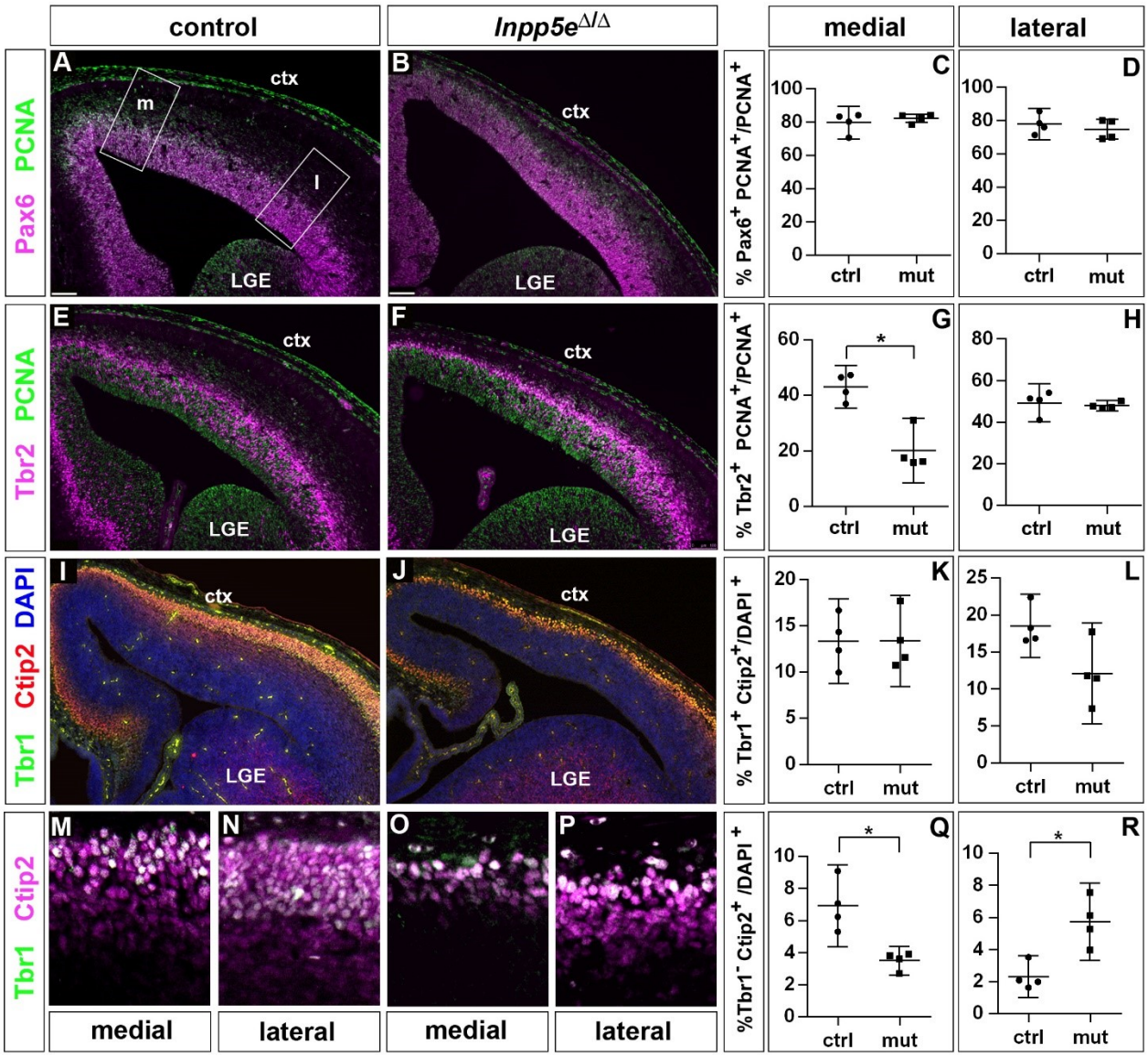

Figure 2: Proportions of radial glial cells, basal progenitors and neurons in the neocortex of E14.5 *Inpp5e*$^{\Delta/\Delta}$ embryos. (A-D) The proportion of radial glial cells remains unaffected by the *Inpp5e* mutation as revealed by Pax6/PCNA double immunofluorescence. The boxes in A indicate the regions in the medial (m) and lateral (l) telencephalon at which cell counts were performed. (E-H) Tbr2/PCNA double staining showed a reduced proportion of basal progenitors in the *Inpp5e*$^{\Delta/\Delta}$ medial but not lateral neocortex. (I-R) Neuron formation in the *Inpp5e*$^{\Delta/\Delta}$ mutant necocortex. The proportion of Tbr1^{+}Ctip2^{+} neurons is not significantly altered (I-L) whereas the proportion of Tbr1^{-}Ctip2^{+} neurons is decreased and increased in the medial and lateral neocortex, respectively (M-R). All statistical data are presented as means ± 95% confidence intervals (CI); Mann Whitney tests; n = 4; * $p < 0.05$. Scale bars: 100μm (A) and 50μm (M). ctx: cortex; LGE: lateral ganglionic eminence.

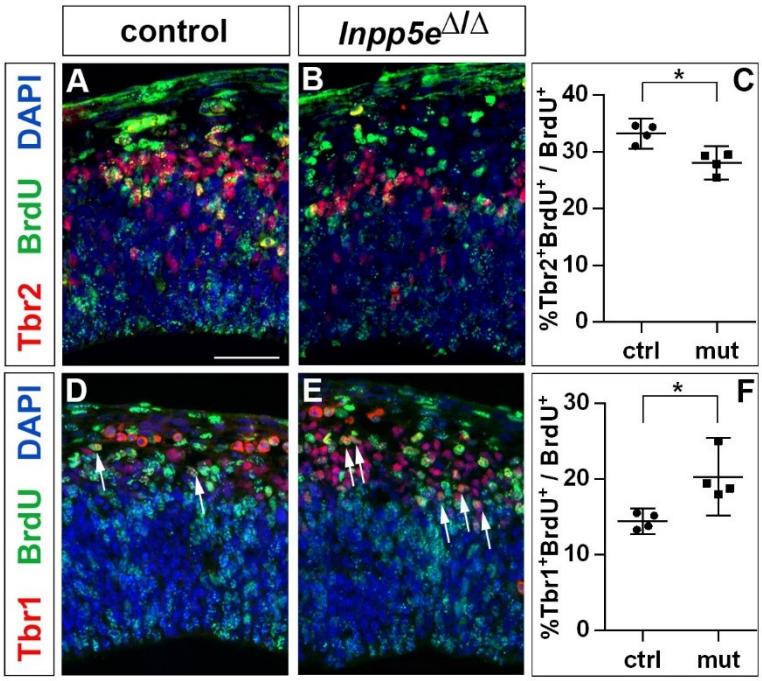

874

875 **Figure 3: Increased neurogenesis at the expense of basal progenitor formation in E12.5**
876 ***Inpp5e*$^{\Delta/\Delta}$ mutants.** Immunohistochemistry on sections of E12.5 control (A, D) and *Inpp5e*$^{\Delta/\Delta}$
877 embryos (B, E) that were treated with BrdU 24 hours earlier. (A-C) Tbr2/BrdU double labelling
878 showed that less basal progenitors formed from the BrdU labelled progenitor cohort. (D-F) The
879 proportion of newly formed Tbr1$^+$ neurons is increased. The arrows in D and E label Tbr1$^+$BrdU$^+$
880 cells. All statistical data are presented as means ± 95% confidence intervals (CI); Mann Whitney
881 tests; n = 4; * $p < 0.05$. Scale bar: 50μm.
882

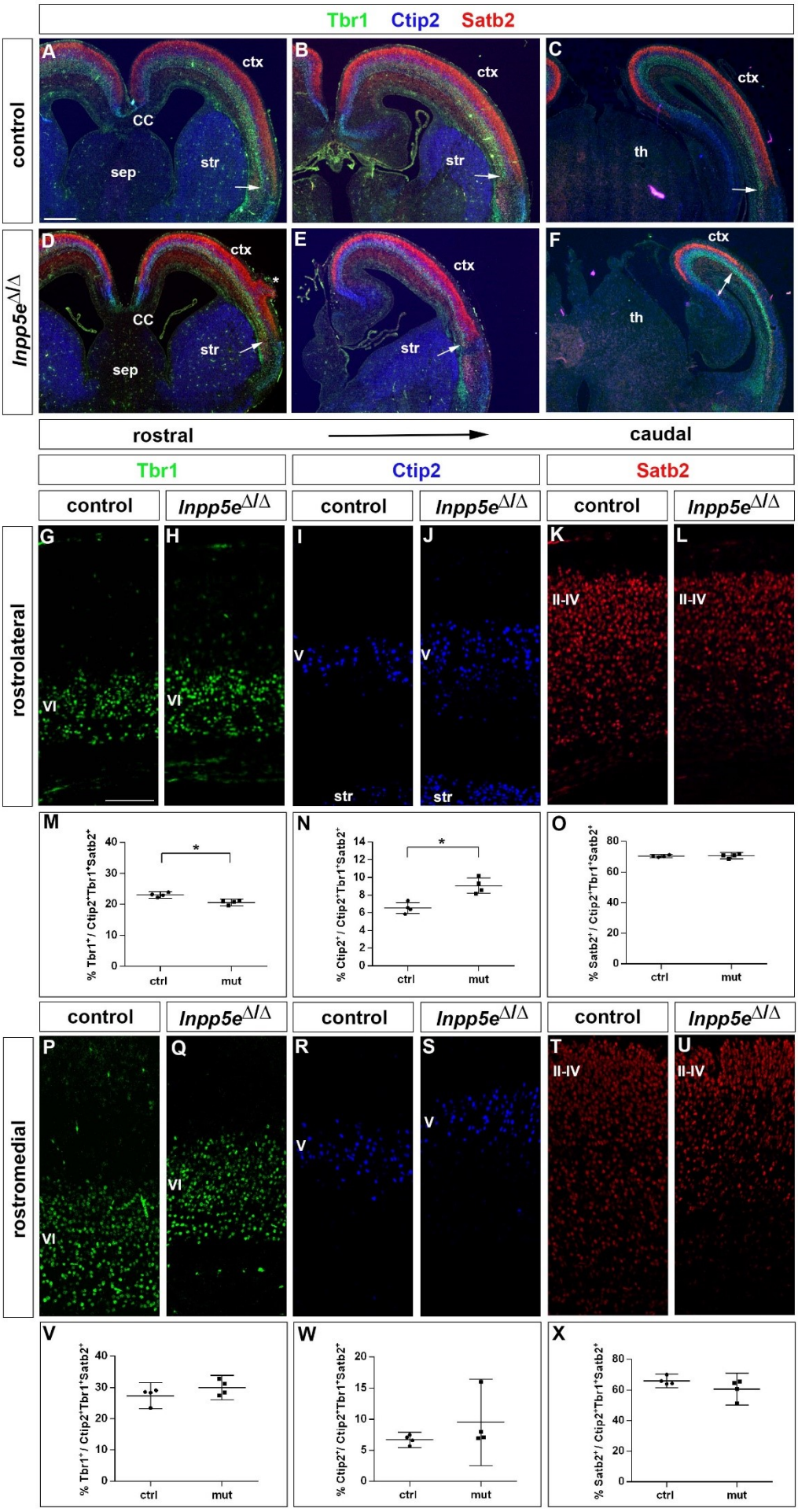
Tbr1 Ctip2 Satb2
control
Inpp5eΔ/Δ
A
B
C
D
E
F
ctx
CC
sep
str
th
rostral
caudal
Tbr1
Ctip2
Satb2
control
Inpp5eΔ/Δ
rostrolateral
rostromedial
G
H
I
J
K
L
M
N
O
P
Q
R
S
T
U
V
W
X
VI
V
II-IV
% Tbr1+ / Ctip2+Tbr1+Satb2+
% Ctip2+ / Ctip2+Tbr1+Satb2+
% Satb2+ / Ctip2+Tbr1+Satb2+
ctrl
mut

883

884 **Figure 4: Increased formation of layer V neurons in E18.5 *Inpp5e*$^{\Delta/\Delta}$ mutants**. (A-F) Coronal
885 sections immunostained for the deep layer markers Tbr1 (layer VI) and Ctip2 (layer V) and for the
886 upper layer marker Satb2 (layers II-IV); there is no obvious defect in layering in the *Inpp5e*$^{\Delta/\Delta}$ mutant
887 except for the formation of a heterotopia (asterisk in D). At caudal levels, the cortex becomes thinner
888 and the rhinal fissure is shifted medially as indicated by the arrows. (G-O) Formation of cortical
889 neurons at rostrolateral levels. The proportion of Tbr1+layer VI neurons is decreased with a
890 concomitant increase in Ctip2+layer V neurons. (P-X) Portion of cortical neurons at rostromedial
891 levels. Immunolabeling with cortical layer markers revealed no significant difference. Note that due
892 to the thinner cortex, the position of layer VI Tbr1+ (Q) and layer V Ctip2+ neurons (J, S) appears to
893 be shifted to more superficial positions, however, the relative order of these layers remains
894 unaffected. All statistical data are presented as means ± 95% confidence intervals (CI); Mann
895 Whitney tests; n = 4; * $p < 0.05$. Scale bars: 500μm (A) and 100μm (G). CC: corpus callosum; ctx:
896 cortex; sep: septum; str: striatum.
897

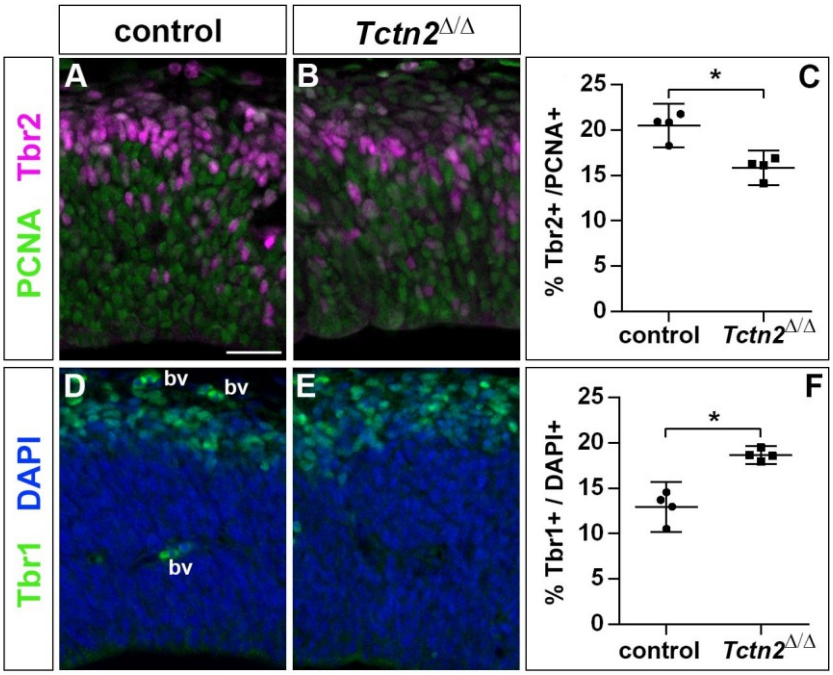

898

899 **Figure 5: Increased generation of cortical neurons in E12.5 *Tctn2*$^{-/-}$ embryos**. (A-C) Double
900 immunofluorescence for PCNA and Tbr2 revealed a significantly decreased proportion of basal
901 progenitors. (D-F) The portion of Tbr1^{+} cortical neurons is increased. All statistical data are presented
902 as means ± 95% confidence intervals (CI); Mann Whitney tests; n = 4; * $p < 0.05$. Scale bar: 50μm.
903 bv: blood vessel.

904

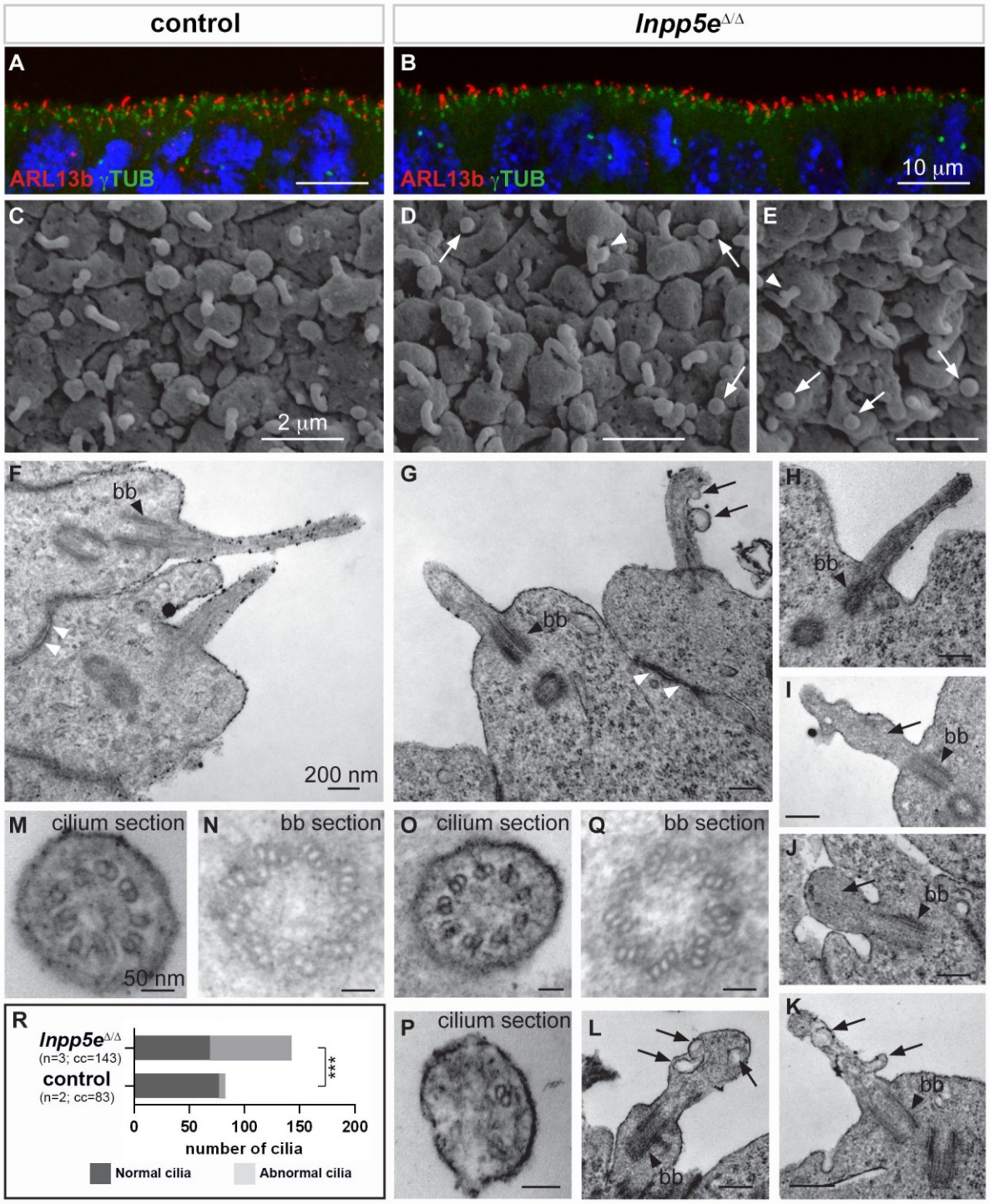

Figure 6: Ciliary defects in E12.5 *Inpp5e*$^{\Delta/\Delta}$ forebrain. (A-B) Immunohistochemistry for Arl13b and γ-Tubulin (γTUB) on E12.5 brain cryosections showed an accumulation of ciliary axonemes and basal bodies, respectively, at the apical border of radial glial cells facing the ventricules in both control (A) and *Inpp5e*$^{\Delta/\Delta}$ (B) embryos without any obvious difference. Scale bars: 10 μm.

(C-E) Scanning electron microscopy (SEM) on E12.5 control (C) and *Inpp5e*$^{\Delta/\Delta}$ (D, E) brains highlighted the presence of primary cilia projecting from the apical surface of radial glial cells in both control (A) and *Inpp5e*$^{\Delta/\Delta}$ (B) embryos. However, SEM also revealed the presence of abnormal cilia

913 in *Inpp5e*$^{\Delta/\Delta}$ embryos having a spherical shape (arrows in D and E) or aberrant lateral buddings
914 (arrowheads in D and E). Scale bars: 2 μm.
915 (F-L) Transmission electron microscopy (TEM) analysis on E12.5 brains showed longitudinal
916 sections of primary cilia in control (F) and *Inpp5e*$^{\Delta/\Delta}$ (G-L) embryos. In control primary cilia, the
917 axoneme appeared as an extension of the basal body (bb, black arrowheards) (F-H). In addition to
918 cilia with normal morphology, abnormal cilia were identified in *Inpp5e*$^{\Delta/\Delta}$ embryos thanks to the
919 presence of a basal body apparently correctly docked to the apical membrane. Abnormal cilia lacked
920 an axoneme (I, J, L) or showed unusual membranous structures, such as budding (G, K) or internal
921 (I, K, L) vesicles (arrows) or undulating peripheral membranes (I). Note that tight junctions (white
922 arrowheads in F and G) appeared normal in *Inpp5e*$^{\Delta/\Delta}$ (G) and control (F) embryos, suggesting that
923 apico-basal polarity of *Inpp5e*$^{\Delta/\Delta}$ radial glial cells was not compromised. Scale bars: 200 nm.
924 (M-Q) TEM images showing transverse sections of the axoneme (M, O, P) and the basal body (N,
925 Q) in control (M, N) and *Inpp5e*$^{\Delta/\Delta}$ (O-Q) embryos with no major difference in the basal bodies
926 between control (N) and *Inpp5e*$^{\Delta/\Delta}$ (Q) embryos. However, transverse section of primary cilia in
927 *Inpp5e*$^{\Delta/\Delta}$ brains revealed the presence of normal axonemes composed of 9 correctly organized
928 doublets of microtubules on some radial glial cells (O), while others harboured an abnormal axoneme
929 containing a lower number of microtubule doublets (P). Scale bars: 50 nm. (R) Graph showing the
930 number of normal versus abnormal cilia (cil.) found on TEM images from control (n=3) or *Inpp5e*$^{\Delta/\Delta}$
931 (n=3) embryos. cc: counted cilia.
932

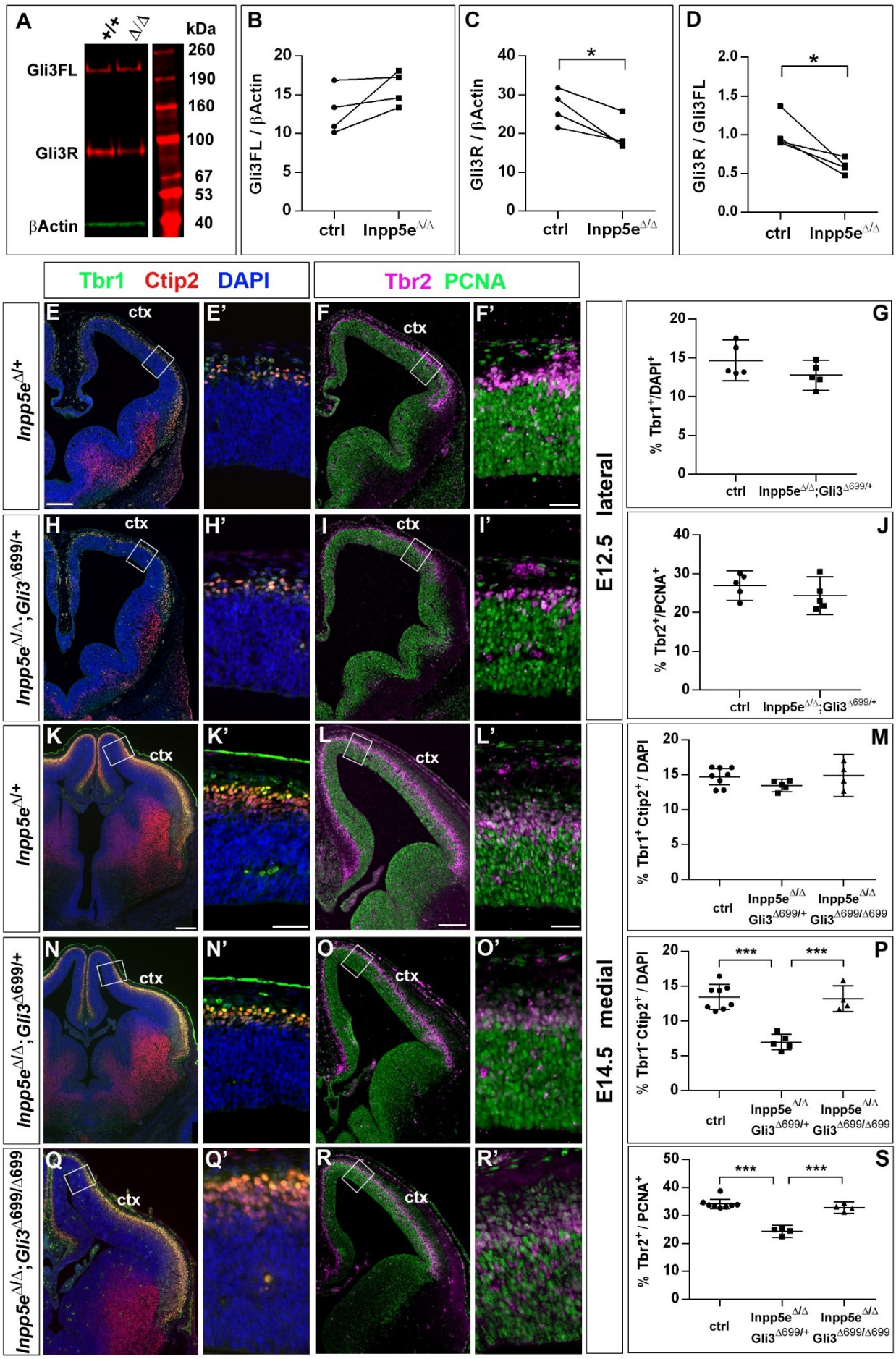
A
+/+
Δ/Δ
kDa
Gli3FL
Gli3R
βActin
260
190
160
100
67
53
40
B
Gli3FL / βActin
ctrl
Inpp5e Δ/Δ
C
Gli3R / βActin
*
D
Gli3R / Gli3FL
Tbr1 Ctip2 DAPI
Tbr2 PCNA
Inpp5e Δ/+
Inpp5e Δ/Δ;Gli3 Δ699/+
Inpp5e Δ/Δ;Gli3 Δ699/Δ699
E12.5 lateral
E14.5 medial
ctx
% Tbr1+/DAPI+
% Tbr2+/PCNA+
% Tbr1+ Ctip2+ / DAPI
% Tbr1- Ctip2+ / DAPI
% Tbr2+ / PCNA+
***

933

934 **Figure 7: Re-introducing the Gli3 repressor rescues the neurogenesis defect in *Inpp5e***
935 **mutants**. (A-D). Gli3 Western blot on E12.5 dorsal telencephalic tissue revealed the Gli3 full length
936 (FL) and repressor (R) forms (A). While Gli3FL levels are not affected (B), levels of Gli3R (C) and
937 the Gli3R/Gli3FL ratio (D) are decreased in *Inpp5e*$^{\Delta/\Delta}$ embryos. A paired t-test was used to evaluate
938 levels of Gli3FL and Gli3R and the Gli3R/Gli3FL ratio in four control/*Inpp5e*$^{\Delta/\Delta}$ embryo pairs derived
939 from four different litters. (E-S) Formation of basal progenitors and neurons in the neocortex of
940 *Inpp5e*$^{\Delta/\Delta}$;Gli3$^{\Delta699/+}$ and *Inpp5e*$^{\Delta/\Delta}$;Gli3$^{\Delta699/699}$ embryos. (E-N) In the lateral neocortex of E12.5
941 embryos, there is no significant difference in the proportions of Tbr1+ neurons (E-G) and basal
942 progenitor cells (H-J) between control and *Inpp5e*$^{\Delta/\Delta}$;Gli3$^{\Delta699/+}$ embryos. (K-S) In the E14.5 medial
943 neocortex, the proportion of Tbr1^{-}Ctip2^{+} neurons (P) and basal progenitors (S) are significantly
944 reduced in *Inpp5e*$^{\Delta/\Delta}$;*Gli3*$^{\Delta699/+}$ embryos but not in *Inpp5e*$^{\Delta/\Delta}$;Gli3$^{\Delta699/699}$ embryos. All statistical data
945 except for the Western blot data (C, D) are presented as means ± 95% confidence intervals (CI);
946 Mann Whitney (n=5) (G, J) and ONE way ANOVA followed by Tukey's multiple comparison test (J,
947 M, P); * $p < 0.05$; ** $p < 0.01$; *** $p < 0.001$. Scale bars: 50μm (E, K, L), 100μm (A), and 250μm (F',
948 K', L'). ctx: cortex; MGE: medial ganglionic eminence; LGE: lateral ganglionic eminence.
949

Supplementary Figure 1: Formation of the telencephalic boundaries in *Inpp5e*$^{\Delta/\Delta}$ embryos. (A-F) Formation of the corticoseptal boundary. Expression of the dorsal marker gene *Pax6* (A, B, D, E) and of the ventral marker gene *Dlx2* (C, F) remain restricted to the cortex and septum, respectively, with a sharp expression boundary between both tissues. (G-L) Formation of the pallial/subpallial boundary. While there is a sharp expression boundary between cortex and lateral ganglionic eminence (LGE) in wild-type embryos (G-I), scattered Pax6 and *Dlx2* expressing cells (arrows in J and K) are found in the mutant LGE and cortex, respectively, while the *Dbx1* expression domain characteristic of the ventral pallium (VP) is fuzzier (L). CGE: caudal ganglionic eminence; ctx: cortex; MGE: medial ganglionic eminence; sep: septum; th: thalamus. Scale bars: 200μm.

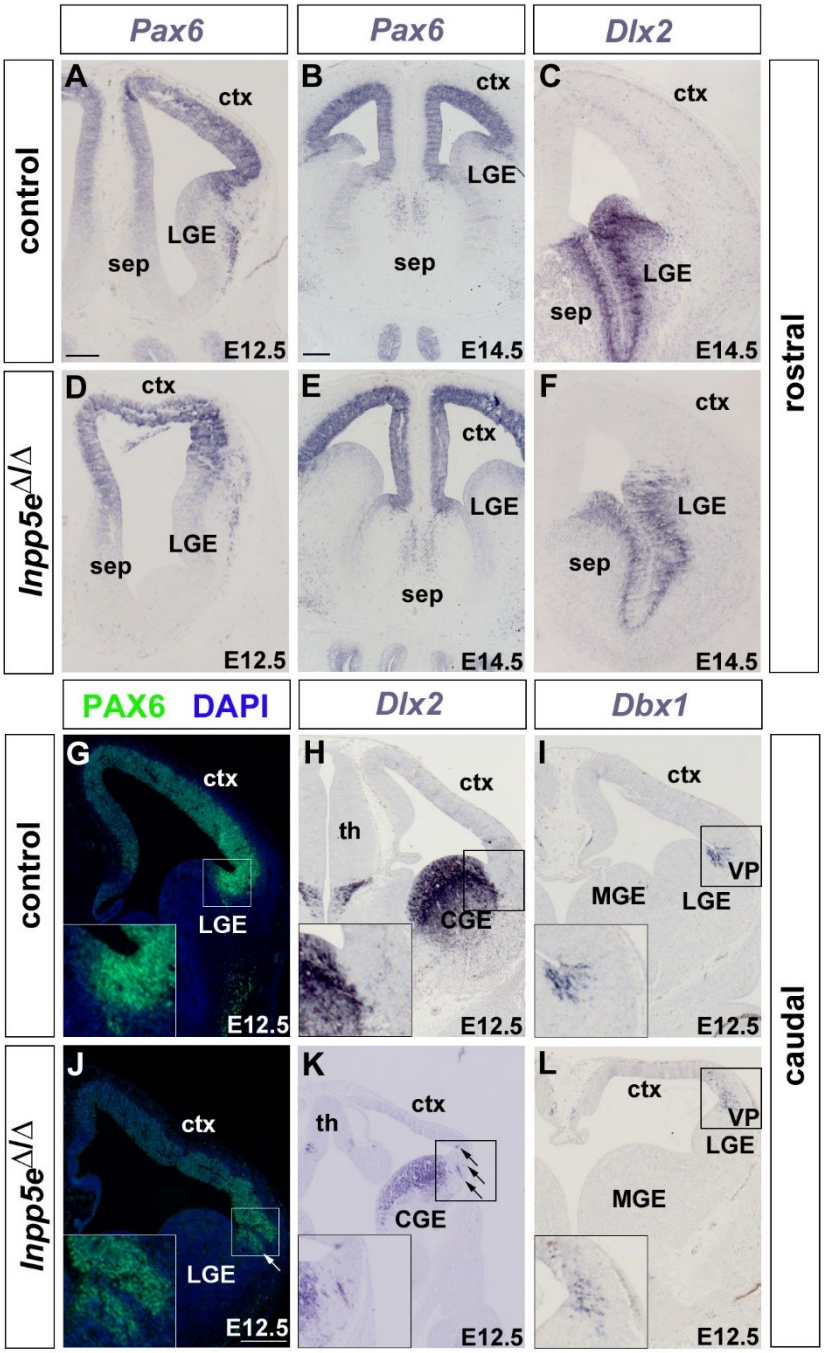

Supplementary Figure 2: Wnt/β-catenin and Bmp signalling in the dorsomedial telencephalon of E12.5 *Inpp5e*$^{\Delta/\Delta}$ embryos. (A, B, E, F) Reduced Wnt/β-catenin signalling in *Inpp5e*$^{\Delta/\Delta}$ embryos. (A, E) *Wnt2b* expression is confined to the cortical hem (h) while there are only few scattered Wnt2b expressing cells in the mutant. (B, F) Graded expression of the Wnt target gene *Axin2* in the dorsal midline is reduced in mutant embryos. (C, D, G, H) Roof plate (rp) expression of *Bmp4* and its target gene *Msx1* are reduced in *Inpp5e*$^{\Delta/\Delta}$ embryos. Scale bar: 100μm.

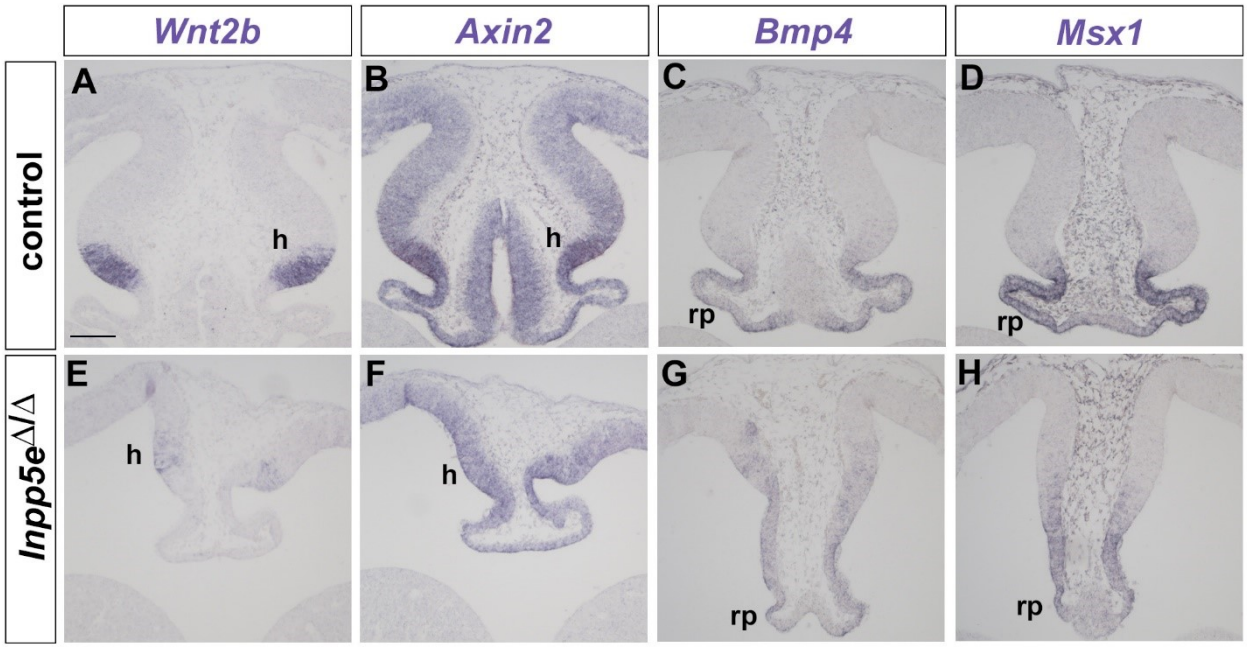

Supplementary Figure 3: Expression of cortical progenitor markers in *Inpp5e*$^{\Delta/\Delta}$ embryos. (A-J) Dorsal marker gene expression at patterning stages (E12.5). *Emx1*, *Lhx2*, *Pax6* and *Ngn2* are still expressed in the developing neocortex of *Inpp5e*$^{\Delta/\Delta}$ embryos though the *Lhx2* medial to lateral (B, C, G, H) and the *Pax6*/*Ngn2* lateral to medial (D, E, I, J) expression gradients are flatter. (K-T) Neocortical progenitors express *Lhx2*, *Pax6* and *Ngn2* in E14.5 *Inpp5e*$^{\Delta/\Delta}$ embryos. Note the folding of the neocortex at caudal levels (arrows in P, R and T). CGE: caudal ganglionic eminence; ctx: cortex; MGE: medial ganglionic eminence; LGE: lateral ganglionic eminence; pt: prethalamus; sep: septum; th: thalamus. Scale bars: 200μm.

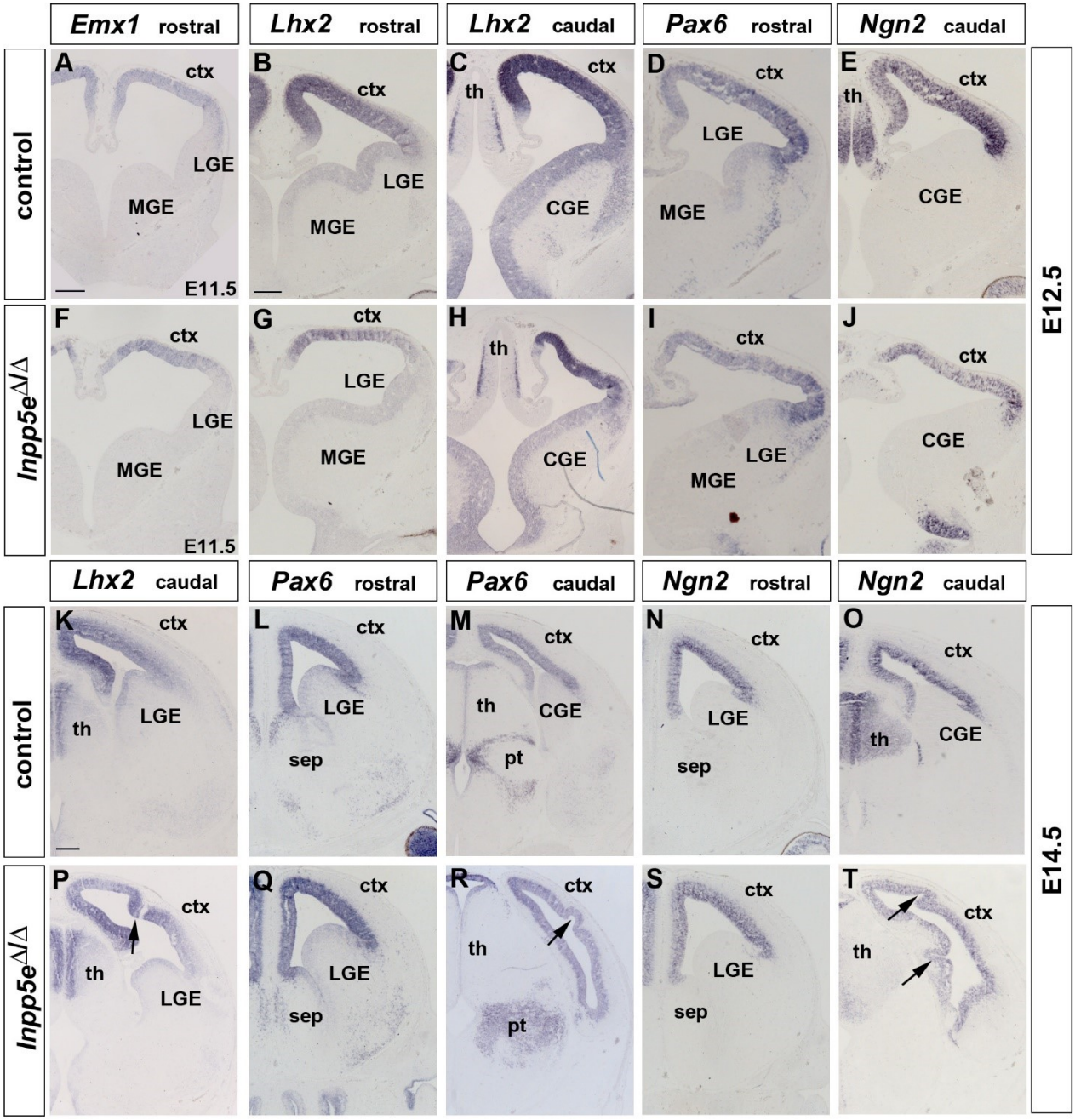

Supplementary Figure 4: Proportion of mitotic progenitors in *Inpp5e*$^{\Delta/\Delta}$ embryos. (A-H) Proportions of mitotic progenitors in E12.5 control (A, E) and *Inpp5e*$^{\Delta/\Delta}$ embryos (B, F) as revealed by pHH3 (mitotic cells) and PCNA (all progenitor cells) double immunofluorescence. Note the reduction in mitotic basal progenitors in the *Inpp5e*$^{\Delta/\Delta}$ medial neocortex (A, B, D). (I-P) The proportions of apical and basal progenitors is not significantly different in E14.5 control and *Inpp5e*$^{\Delta/\Delta}$ embryos. In all panels, radial glia cells divide at the ventricular surface whereas mitotic basal progenitors locate in abventricular positions. All statistical data are presented as means ± 95% confidence intervals (CI); Mann Whitney tests; n = 4; * $p < 0.05$. Scale bar: 50μm.

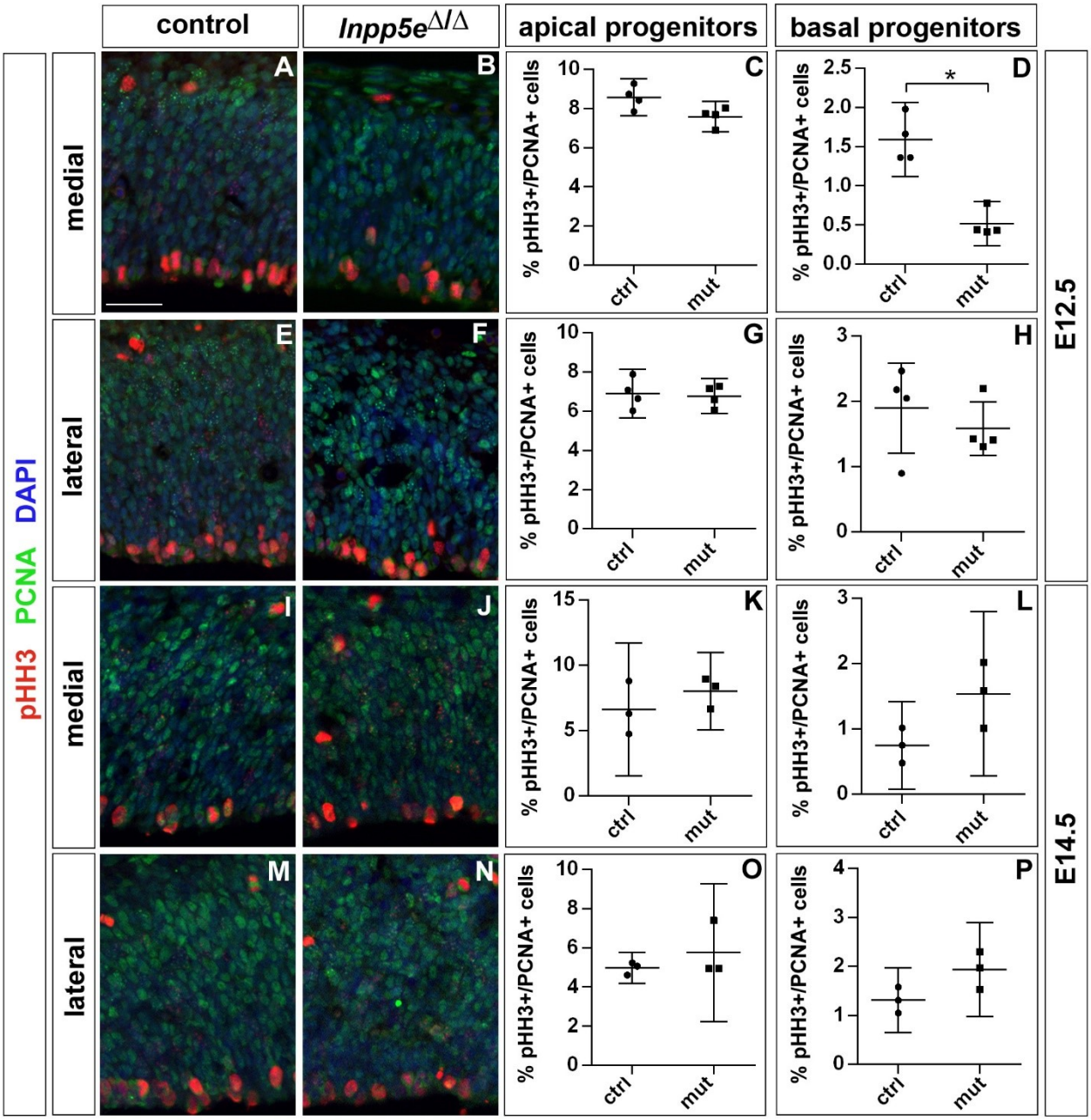

Supplementary Figure 5: Cell cycle of cortical progenitors in E12.5 *Inpp5e*$^{\Delta/\Delta}$ embryos. (A) Schematic illustrating the BrdU/IdU double labelling strategy to measure S phase (T_S) and total cell cycle length (T_C). 90 minutes after an initial IdU administration, pregnant females received an intraperitoneal BrdU injection. Embryos are harvested 30 minutes later. (B, C) Double immunofluorescence to detect IdU+ and BrdU+ progenitors. (D) Quantification showing no significant change in T_S and T_C. Statistical data are presented as means ± 95% confidence intervals (CI); Mann Whitney tests; n = 4; * $p < 0.05$. Scale bar: 50μm.

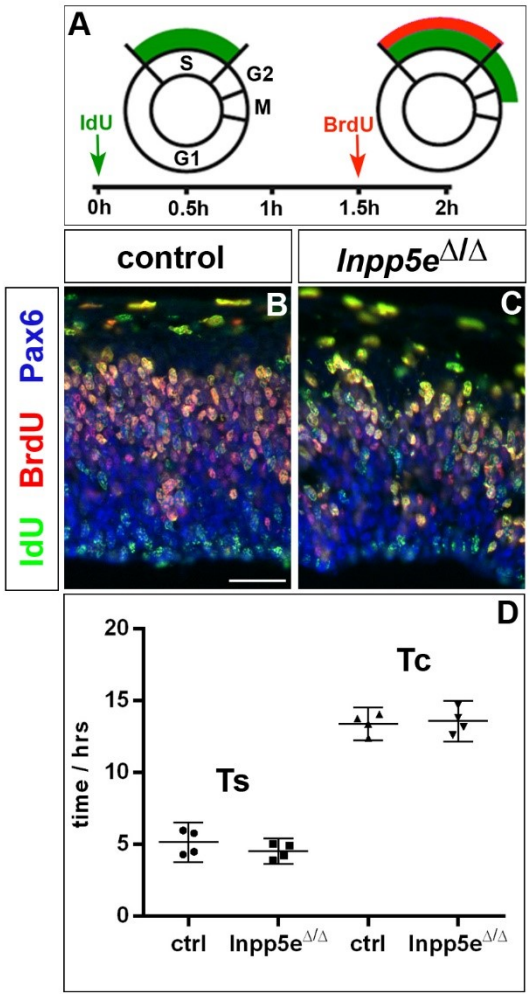

Supplementary Figure 6: Whole mount preparations of E18.5 brains. (A) Control. (B) *Inpp5e*$^{\Delta/\Delta}$ brain. Note the absence of obvious protrusions of the olfactory bulbs (ob) in the mutant. Ctx: cortex. Scale bar: 1 mm.

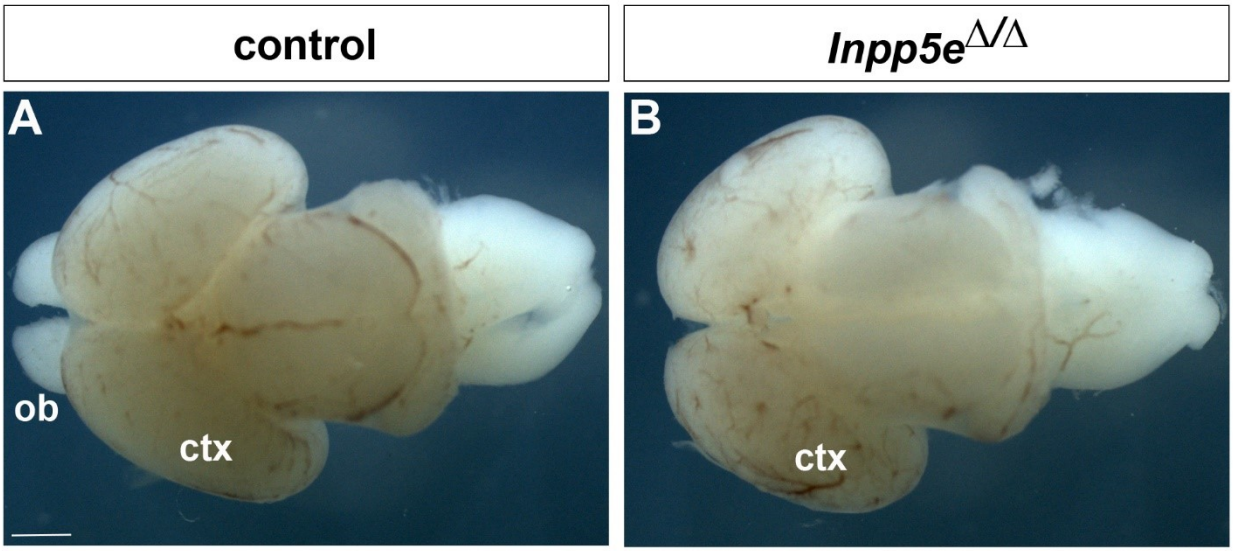

Supplementary Figure 7: Forebrain malformations in E18.5 *Inpp5e*$^{\Delta/\Delta}$ embryos. (A-F) Coronal sections through the forebrain of E18.5 control (A-C) and *Inpp5e*$^{\Delta/\Delta}$ (D-F) embryos. The asterisk in (D) demarcates a heterotopia in the *Inpp5e* mutant. Note that the mutant lateral neocortex is thinner at intermediate and caudal levels (E, F). The lines in (A) indicate where cortical thickness was measured at medial (m) and lateral (l) levels. (G, H) Quantification of cortical thickness. CC: corpus callosum; ctx: cortex; hip: hippocampus; sep: septum; str: striatum; th: thalamus. Scale bar: 500μm. Statistical data are presented as means ± 95% confidence intervals (CI); Two way ANOVA followed by Sidak multiple comparisons test; n = 4; * $p < 0.05$; ** $p < 0.005$; *** $p < 0.001$.

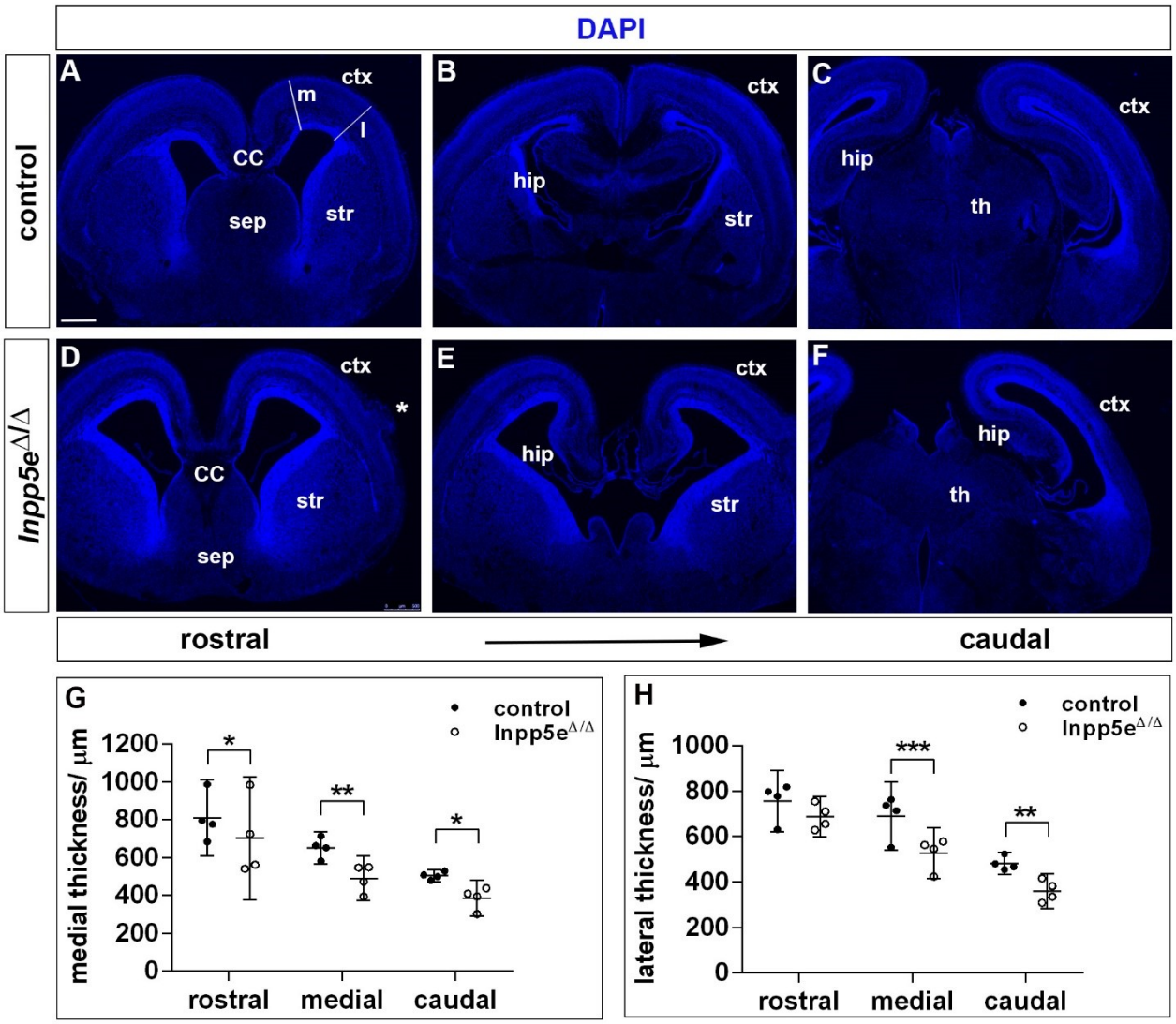

Supplementary Figure 8: Hippocampus formation in *Inpp5e*$^{\Delta/\Delta}$ embryos. (A-F) Hippocampal marker gene expression in E18.5 control (A-C) and *Inpp5e*$^{\Delta/\Delta}$ embryos (D-F). Expression of *Nrp2* labels the whole hippocampal formation (A), while *Scip1* is expressed in CA1 and in the neocortex (B). Prox1 expression is confined to the dentate gyrus (DG) (C). In *Inpp5e*$^{\Delta/\Delta}$ embryos, these hippocampal markers are expressed but their expression domains are severely reduced or disorganized (D-F).

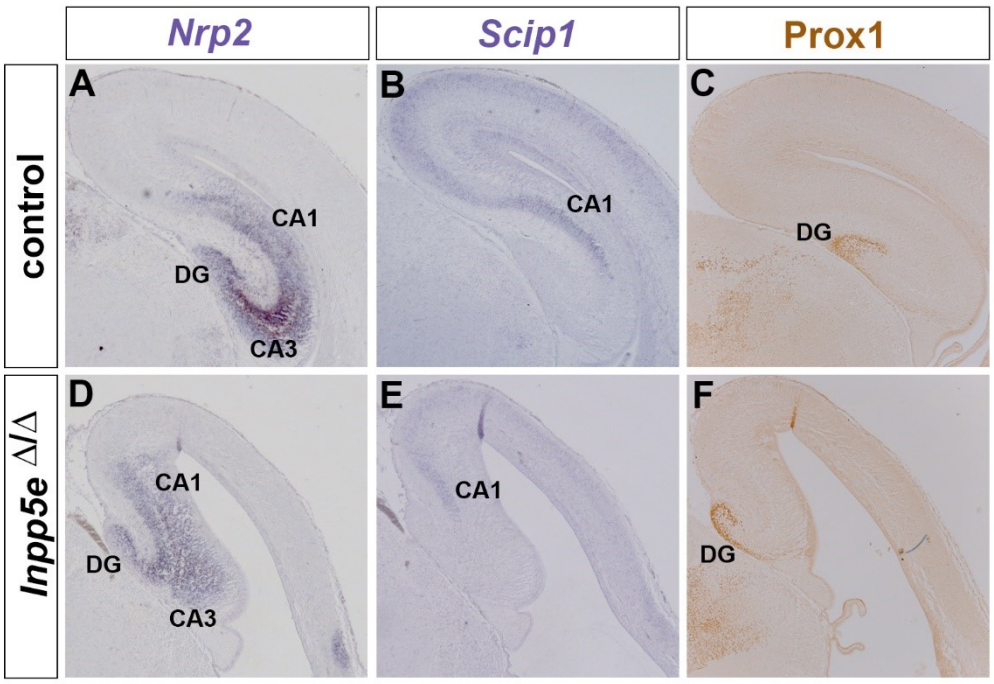

Supplementary Figure 9: Formation of the corpus callosum in E18.5 *Inpp5e*$^{\Delta/\Delta}$ embryos. (A, B) Coronal section through the telencephalon stained with L1 and GFAP to reveal the corpus callosum (CC) and glial cells, respectively. The corpus callosum is smaller in *Inpp5e*$^{\Delta/\Delta}$ embryos while the glial wedge (GW), the induseum griseum glia (IGG) and the midline zipper glia (MZG) occupy their correct position surrounding the corpus callosum. (C) Quantification of corpus callosum thickness. Statistical data are presented as means ± 95% confidence intervals (CI); Mann Whitney tests; n = 4; * $p < 0.05$. Scale bar: 250μm.

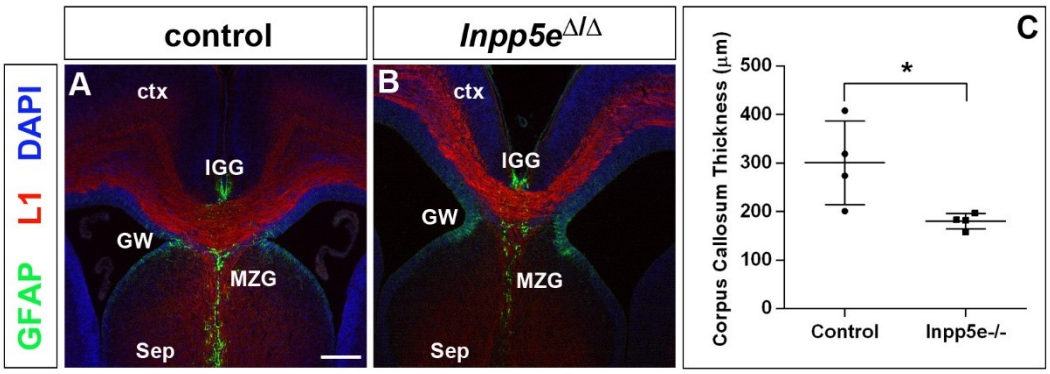

Supplementary Figure 10: Erk signalling in *Inpp5e*$^{\square/\square}$ embryos. (A, E) Western blot analysis on dorsal telencephalic tissue from E12.5 (A) and E14.5 (E) embryos using anti-phosphoErk$^{T202/Y204}$ and total-Erk antibodies. (B, F) Quantification of the Western blots. A paired t-test was used to evaluate relative pErk/Erk expression levels in four control/*Inpp5e*$^{\square/\square}$ embryo pairs derived from four different litters; statistical data are presented as means ± 95% confidence intervals (CI). (C, D, G, H) Immunohistochemistry for phosphoErk$^{T202/Y204}$ on coronal sections of the telencephalon of E12.5 (C, D) and E14.5 (G, H) embryos. ctx: cortex; MGE: medial ganglionic eminence; LGE: lateral ganglionic eminence; th: thalamus Scale bars: 100 μm.

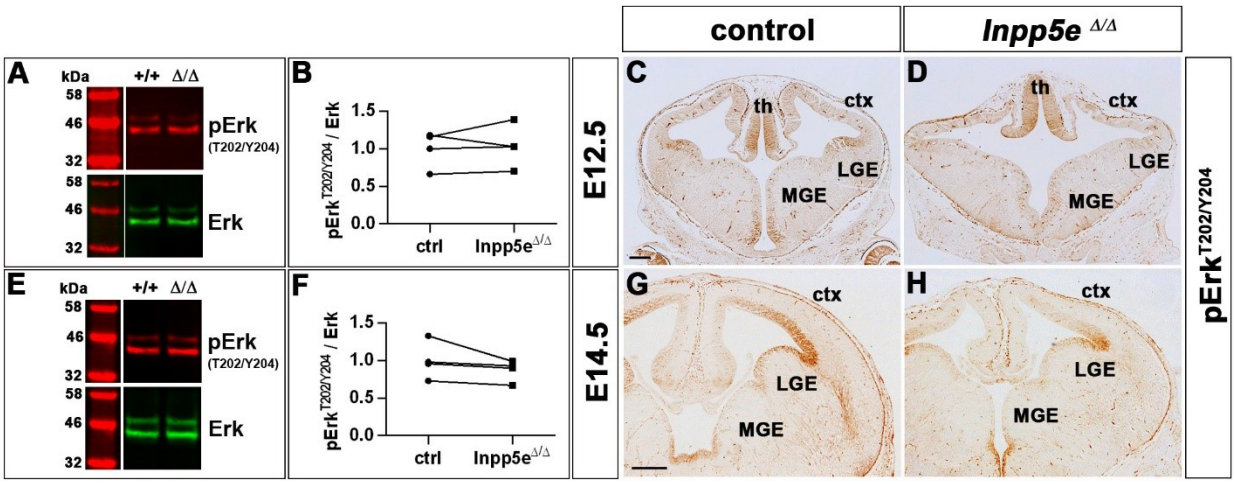

Supplementary Figure 11: Akt and mTOR signalling in *Inpp5e*$^{\Delta/\Delta}$ embryos. (A, E) Western blot analyses on dorsal telencephalic tissue from E12.5 (A, C, E) and E14.5 (B, D, F) embryos with the indicated antibodies. (A, B) Increased ratio of pAkt^{S473}/total Akt in E12.5 *Inpp5e*$^{\Delta/\Delta}$ embryos but not at E14.5. (C, D) Phosphorylation of S6 at residues S235/S236 is increased in the dorsal telencephalon of E12.5 and E14.5 *Inpp5e*$^{\Delta/\Delta}$ embryos. (E, F) E12.5 *Inpp5e*$^{\Delta/\Delta}$ embryos show an increased phosphorylation of S6 at residues S240/S244. (G-P) *Inpp5e*$^{\Delta/\Delta}$ embryos treated with rapamycin show an augmented proportion of Tbr1+ neurons (G-J, O) and a reduced proportion of Tbr2+ basal progenitors (K-N, P). For quantification of the Western blots, paired t-test were used to evaluate expression levels of the phosphorylated versus unphosphorylated proteins in four control/*Inpp5e*$^{\Delta/\Delta}$ embryo pairs derived from four different litters. Immunofluorescence stainings were analysed by Mann Whitney tests. Statistical data are presented as means ± 95% confidence intervals (CI); n = 4; * $p < 0.05$; *** $p < 0.005$.

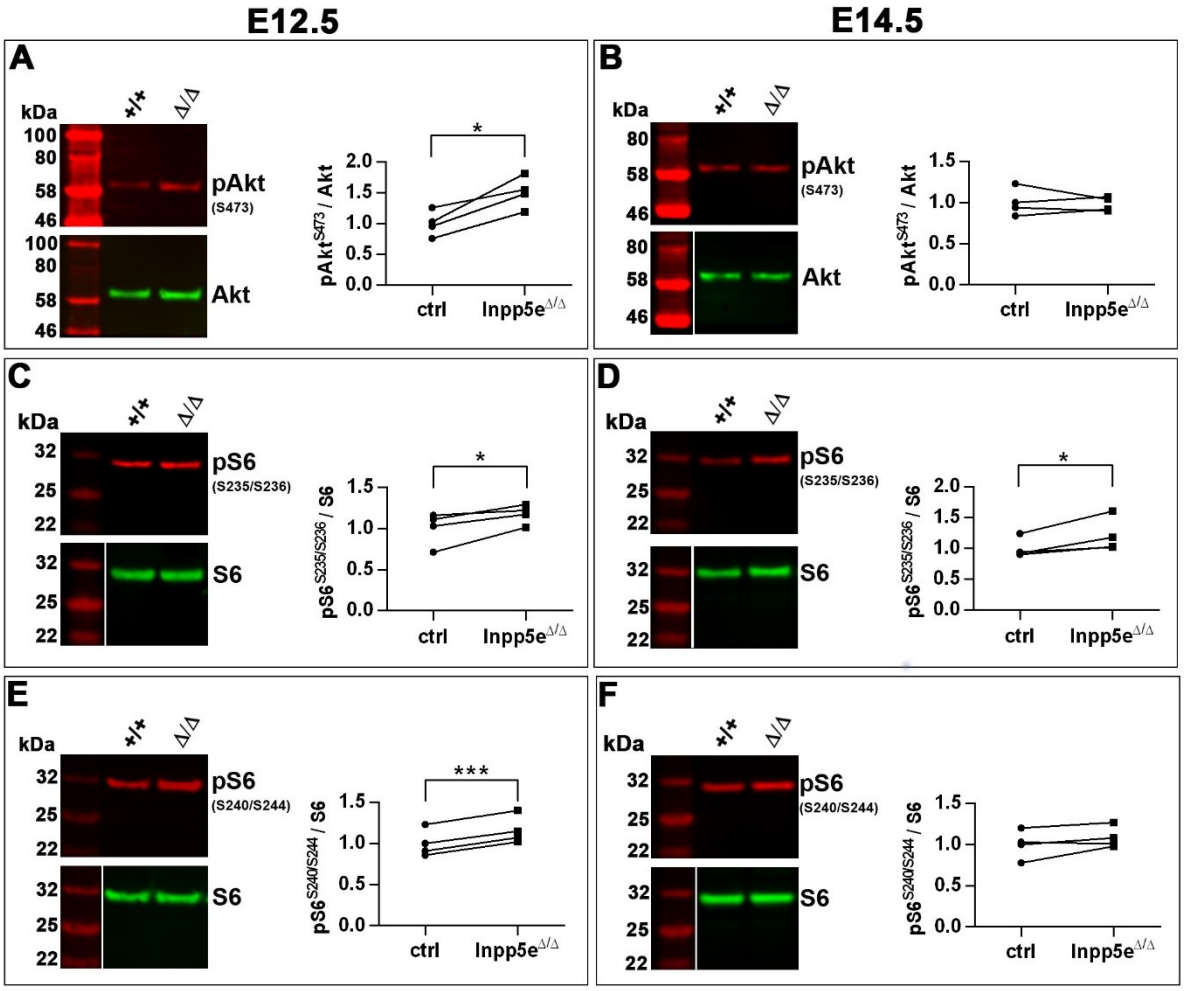
E12.5
E14.5
A
B
C
D
E
F
kDa
+/+
Δ/Δ
pAkt
(S473)
Akt
pS6
(S235/S236)
(S240/S244)
S6
pAkt^S473 / Akt
pS6^S235/S236 / S6
pS6^S240/S244 / S6
ctrl
Inpp5e^Δ/Δ

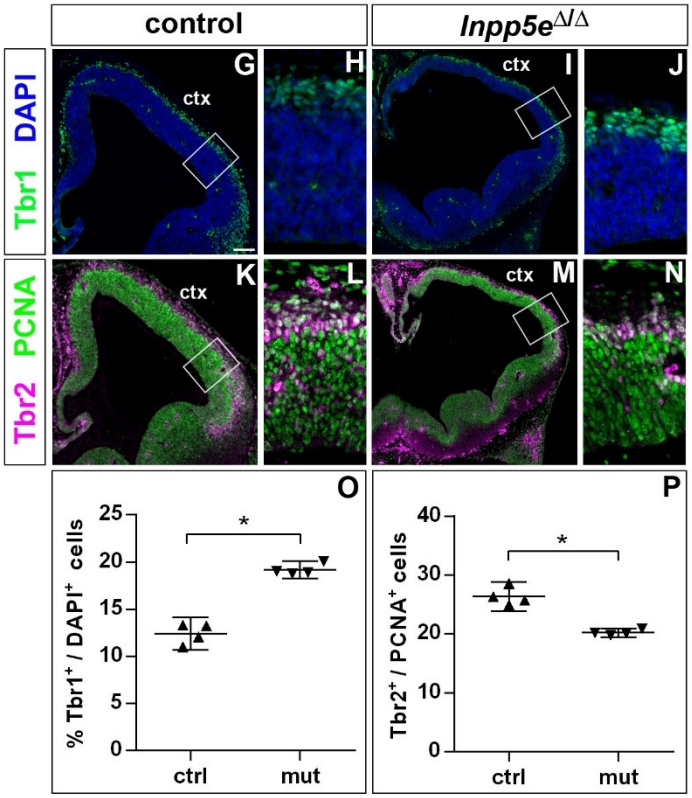
control
Inpp5e^Δ/Δ
DAPI
Tbr1
PCNA
Tbr2
ctx
G
H
I
J
K
L
M
N
O
P
% Tbr1+ / DAPI+ cells
Tbr2+ / PCNA+ cells
ctrl
mut

Supplementary Figure 12: *Gli3* mRNA expression in Inpp5e mutants. (A, B) *Gli3* in situ hybridization showing *Gli3* mRNA expression in the cortex (ctx) and lateral ganglionic eminence (LGE) of control (A) and *Inpp5e*$^{\Delta/\Delta}$ embryos (B).

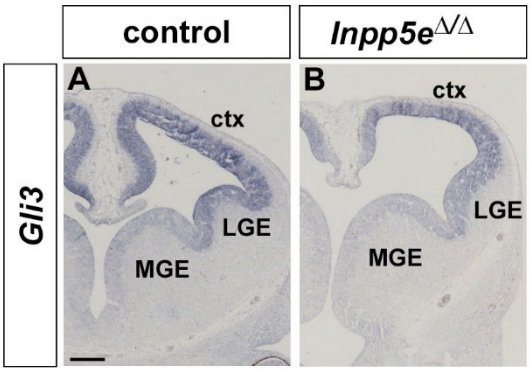

Supplementary Figure 13: Rescue of eye development in *Inpp5e*$^{\Delta/\Delta}$;*Gli3*$^{\Delta699/+}$ embryos. (A-C) Side views of the heads of E12.5 embryos with the indicated genotype. *Inpp5e*$^{\Delta/\Delta}$ embryos lack the eye completely or only form a small remnant whereas eye formation is not affected in *Inpp5e*$^{\Delta/\Delta}$;*Gli3*$^{\Delta699/+}$ embryos. Scale bar: 1mm

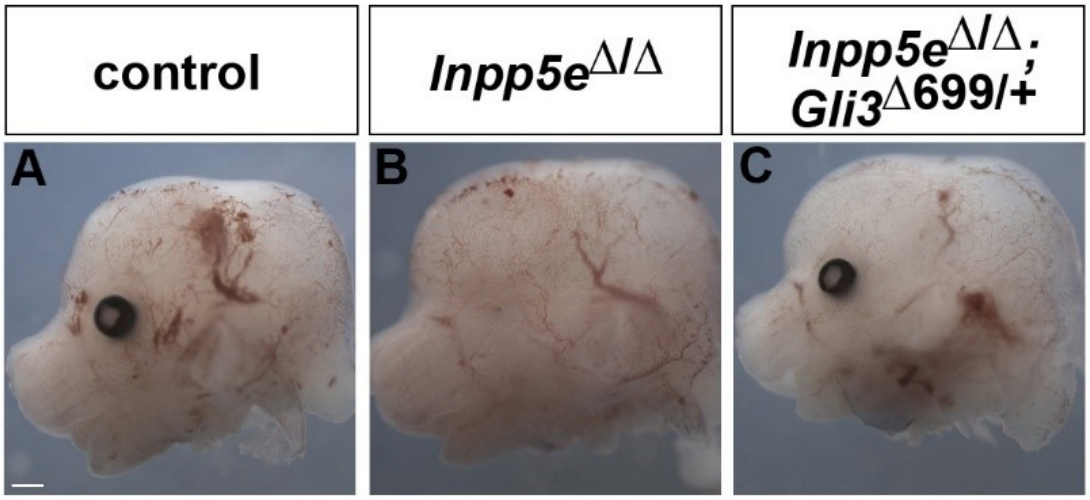
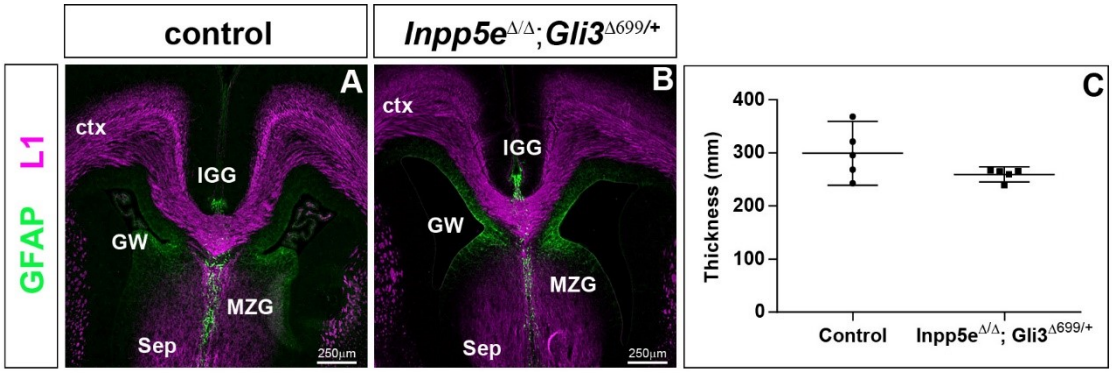
Supplementary Figure 14: Rescue of corpus callosum formation in *Inpp5e*$^{\Delta/\Delta}$;*Gli3*$^{\Delta699/+}$ embryos. (A-B) Coronal section through the telencephalon stained with L1 and GFAP to reveal the corpus callosum (CC) and glial cells, respectively. There is no significant difference in the size of the corpus callosum between control and *Inpp5e*$^{\Delta/\Delta}$;*Gli3*$^{\Delta699/+}$ embryos; the glial wedge (GW), the induseum griseum glia (IGG) and the midline zipper glia (MZG) are formed in their correct position. (C) Quantification of corpus callosum thickness. Statistical data are presented as means ± 95% confidence intervals (CI); Mann Whitney tests; n = 4; Scale bar: 250μm.